Pore and Surface Diffusion in Multicomponent Adsorption and Liquid Chromatography Systems

Z. Ma, R. D. Whitley, and N.-H. L. Wang
School of Chemical Engineering, Purdue University, West Lafayette, IN 47907

A generalized parallel pore and surface diffusion model for multicomponent adsorption and liquid chromatography is formulated and solved numerically. Analytical solution for first- and second-order central moments for a pulse on a plateau input is used as benchmarks for the numerical solutions. Theoretical predictions are compared with experimental data for two systems: ion-exchange of strontium, sodium, and calcium in a zeolite and competitive adsorption of two organics on activated carbon. In a linear isotherm region of single-component systems, both surface and pore diffusion cause symmetric spreading in breakthrough curves. In a highly nonlinear isotherm region, however, surface diffusion causes pronounced tailing in breakthrough curves; the larger the step change in concentration, the more pronounced tailing, in contrast to relatively symmetric breakthroughs due to pore diffusion. If only a single diffusion mechanism is assumed in analyzing the data of parallel diffusion systems, a concentration-dependent apparent surface diffusivity or pore diffusivity results; for a convex isotherm, the apparent surface diffusivity increases, whereas the apparent pore diffusivity decreases with increasing concentration. For a multicomponent nonlinear system, elution order can change if pore diffusion dominates for a low-affinity solute, whereas surface diffusion dominates for a high-affinity solute.

Introduction

Liquid chromatography and adsorption processes have been employed extensively in large scale for chemical and biochemical recovery and purification (Wankat, 1986; Belter et al., 1988; Dechow, 1989; Asenjo, 1990). In most of the large-scale processes, relatively large porous particles (50–1,000 μm in diameter) are used to reduce pressure drop and sorbent cost. Intraparticle diffusion is usually the rate-limiting step in these systems and it controls the sharpness of breakthrough curves and elution bands.

For low-affinity solutes in macroporous sorbents, pore diffusion is usually the dominant intraparticle diffusion mechanism (Furuya et al., 1989). However, many applications require sorbents that have high capacities and high selectivities for the solutes of interest, because recovery and purification of products can be achieved using a small amount of sorbents. Adsorption of organics on activated carbon in waste water treatment is a typical example (Thacker et al., 1984). For a high-affinity solute, surface concentration can be higher than pore concentration by orders of magnitude. Although surface diffusivity is usually smaller than pore diffusivity by one or two orders of magnitude (Suzuki, 1990), a high surface concentration gradient can result in a large surface diffusion flux that is much greater than a pore diffusion flux. If a pore diffusion model is used to estimate pore diffusion coefficients in such systems, the resulting values can be erroneously large, sometimes even larger than Brownian diffusivities for high-affinity solutes. If a single diffusion model is used in analyzing the data of a parallel diffusion system, the resulting diffusion coefficient may depend strongly on feed concentration (Yoshida et al., 1994). Furthermore, in most applications, multiple competing adsorbates are present and they may have different diffusion mechanisms, which affect directly their competitive adsorption and distribution in a column. For these reasons, a multicomponent chromatography model for parameter estimation and scale-up should take into account both diffusion mechanisms in order to be useful for a wide

Correspondence concerning this article should be addressed to N.-H. L. Wang.
R. D. Whitley is currently with Air Products and Chemicals, Inc., Allentown, PA 18195.

Table 1. Key References on Combined Diffusion Model

	Adsorption Isotherms	Sorbent	Adsorbate	No. of Solutes	Mathematical Treatment	Solution Method	Oper. Mode
Masamune et al. (1965)	Linear	—	—	1	Analytical numerical	Analytical	Fix bed frontal
Brecher et al. (1967)	B.E.T.	Silica gel	Organics	1	Numerical	Finite difference	Batch
Schneider and Smith (1968a,b)	Linear	Silica gel	Organics	1	Moment analysis	Analytical	Fix bed pulse
Mansour et al. (1982)	Langmuir Freundlich	Activated carbon	Organics	3	Numerical	Finite difference	Fix bed frontal
Fritz et al. (1980)	Langmuir Freundlich	Activated carbon	Organics	2	Numerical	Finite difference	Batch
Merk et al. (1980)	Langmuir Freundlich	Activated carbon	Organics	2	Numerical	Finite difference	Fix bed frontal
Thacker et al. (1984)	Freundlich IAS	Activated carbon	Organics	2	Numerical	Collocation	Fix bed frontal
Do and Rice (1987)	—	—	—	1	General model formulation	—	—
Yoshida et al. (1994)	Langmuir	Chitosan	BSA	1	Numerical	Finite difference	Batch
Current Work	SPT	Activated carbon	Organics	2	General model formulation	OCFE	Fix bed
	Mass Action	Zeolite	Cs^+ Sr^{++} ions	3	Benchmark numerical against analytical solution		Frontal, pulse, sequential loading

range of applications. Development of such a model and fundamental understanding of the coupled adsorption and intraparticle transport phenomena in multicomponent systems are major goals of this study.

Surface diffusion in gas-phase adsorption systems is well documented, extensively studied, and reviewed by Ruthven (1984) and Kapoor et al. (1989). Compared to gas-phase systems, the mechanism of surface diffusion in liquid-phase adsorption systems is not as well understood, and relatively little data on surface diffusivities are available. This can be attributed to the lack of *in-situ* experimental techniques for determining the intrinsic surface diffusivities of solutes at liquid/solid interfaces. Most studies employ indirect methods in determining surface diffusivities in liquid systems. For example, batch-rotating basket and Wicke–Kallenbach experiments were used to estimate surface diffusivities of organic solutes in activated carbon (Komiyama and Smith, 1974; Suzuki and Takao, 1982). Others have inferred surface diffusivities of organics by matching breakthrough curves with model predictions (Dedrick and Beckmann, 1967; Merk et al., 1980; Thacker et al., 1984). Pulse data have also been used to estimate surface diffusivities of organics in a modified silica gel using moment analysis (Miyabe and Suzuki, 1992). Only recently, direct measurements of surface diffusivity of a protein, bovine serum albumin (BSA) have been achieved using a laser fluorescence technique (Tilton et al., 1990a,b). Other studies in batch adsorption experiments have shown evidence of parallel pore and surface diffusion of BSA in basic chitosan particles (Yoshida et al., 1994), and ion exchange of Cs^+, Sr^{++}, Ca^{++}, and Mg^{++} in zeolites (Robinson et al., 1994).

In the study of intraparticle diffusion, basically three types of models are commonly considered: (1) pore diffusion (Schneider and Smith, 1968a; Berninger et al., 1991); (2) surface diffusion (Crittenden et al., 1980); and (3) pore and surface parallel diffusion in batch adsorption processes (Liapis and Rippin, 1977; Hu and Do, 1994). The key references for parallel diffusion models for both batch and fixed-bed processes are summarized in Table 1. Most of the previous works have focused on interpreting experimental data from batch tests or breakthroughs. Little has been done on the comparison of pore diffusion, surface diffusion, and parallel diffusion in multicomponent chromatography systems.

In this article, a versatile parallel pore and surface diffusion model for multicomponent systems has been formulated and solved numerically for various fixed-bed operations, which include frontal, pulse, and sequential loading. Two analytical solutions for elution of a small pulse are obtained from moment analysis for locally linearized kinetic and isotherm systems. The analytical solutions are used as benchmarks for the numerical solutions in order to ensure accuracy and convergence of the latter. By solving the model equations, we can compare the fundamental chromatography dynamics and breakthrough behavior for pore diffusion, surface diffusion, and parallel diffusion cases. In nonlinear isotherm regions, surface diffusion results in asymmetric and more dispersed breakthrough curves in contrast to symmetric and sharp breakthroughs due to pore diffusion. In a binary system, elution order in breakthrough curves may change if transport of the low-affinity solutes is dominated by pore diffusion, whereas that of the high-affinity solutes is by surface diffusion. Simulations are used to analyze experimental data from two systems—adsorption of two organics on activated carbon for waste water treatment and ion exchange of strontium for nuclear waste treatment. Insight gained from this study will help design experiments to understand the intra-

particle diffusion mechanisms from breakthrough data. Furthermore, the general model and associated simulation program can serve as a useful tool for design, optimization, and scale-up for multicomponent nonlinear systems.

Theory

Before discussing the assumptions needed for model formulation, we first introduce the physical processes considered in this model. Convection along the column axial direction and axial dispersion are the mass transport mechanisms in the bulk phase. Molecules from the bulk interstitial phase are transported via axial convection and Brownian diffusion (film diffusion) onto the particle surface. Inside the particle, molecules can diffuse into the inner portion of a particle via surface diffusion, pore diffusion, or both, while slow adsorption/desorption (nonequilibrium) from the sorbent sites occurs concomitantly. Nonequilibrium adsorption is considered because the intrinsic adsorption or desorption rates of biomolecules can be slow compared to the mass-transfer rates (which include axial convection, film diffusion, and intraparticle diffusion). Their liquid phase and solid phase concentrations cannot be related by equilibrium isotherms, and must be related by intrinsic kinetic equations (Jin et al., 1994).

To formulate a generalized model corresponding to the aforementioned physical processes, we need to make the following assumptions: (1) homogeneous packing; (2) plug flow with constant linear velocity along the column; (3) constant temperature along the column; (4) homogeneous pore size distribution; (5) pore and surface diffusion can occur in parallel with constant diffusion coefficients. In reality, a bed is often packed with polydispersed particles; it has been shown, however, that axial dispersion in a packed bed with polydispersed particles can be modeled as a packed bed with monodispersed particles using an effective axial dispersion coefficient (Yeroshenkova et al., 1983). Resin pellets are often porous with macro- and micropores; previous studies have shown that particles with bidispersed pores can be approximated with homogeneous pore distribution with an effective pore diffusivity (Neogi and Ruckenstein, 1980; Whitaker, 1988). Therefore, a model based on these assumptions is a reasonable approximation for many systems.

Equations for the generalized model

Mass Balance for the Mobile Phase. The transport equation for a solute in the mobile phase in column chromatography has been discussed before (Aris, 1959; Aris and Amundson, 1973; Berninger et al., 1991), and can be given as

$$\frac{\partial c_{bi}}{\partial t} = E_{bi}\frac{\partial^2 c_{bi}}{\partial x^2} - u_0\frac{\partial c_{bi}}{\partial x} - \frac{(1-\epsilon_b)}{\epsilon_b}\frac{3k_{fi}}{R} \times [c_{bi} - c_{pi}(r=R)] \qquad i=1, 2, \ldots, N, \quad (1)$$

where c_{bi} and c_{pi} are the mobile and pore phase concentrations of the ith component, respectively; u_0 is the interstitial linear velocity; E_{bi} is the axial dispersion coefficient, and k_{fi} is the film mass-transfer coefficient. The initial and boundary conditions are written as

$$c_{bi} = c_{bi}(0, x) \qquad i=1, 2, \ldots, N \quad (2a)$$

$$E_{bi}\frac{\partial c_{bi}}{\partial x} = \begin{cases} u_0[c_{bi} - c_{fi}(t)] & x=0 \\ 0 & x=L \end{cases} \qquad i=1, 2, \ldots, N, \quad (2b)$$

where c_{fi} is the inlet concentration of the ith component, and it can be a linear or stepwise function of time, which corresponds to different operation modes, such as frontal, pulse, or sequential loading.

Mass Balance for the Pore Phase. Fickian diffusion is assumed for pore diffusion transport (Schneider and Smith, 1968b; Komiyama and Smith, 1974; Do and Rice, 1987). The mass-balance equation for the pore phase in a spherical particle can then be written as

$$\frac{\partial c_{pi}}{\partial t} = D_{pi}\frac{1}{r^2}\frac{\partial}{\partial r}\left[r^2\frac{\partial c_{pi}}{\partial r}\right] - \frac{1-\epsilon_p}{\epsilon_p}y_{li}, \quad (3)$$

where y_{li} is the net adsorption rate. Its explicit form is described in detail in the section on Adsorption Kinetics. The initial and boundary conditions are

$$c_{pi} = c_{pi}(0, r) \quad (4a)$$

$$\epsilon_p D_{pi}\frac{\partial c_{pi}}{\partial r} + (1-\epsilon_p)D_{si}\frac{\partial q_i}{\partial r} = k_{fi}(c_{bi} - c_{pi}) \qquad r=R \qquad i=1, 2, \ldots, N \quad (4b)$$

$$\frac{\partial c_{pi}}{\partial r} = 0 \qquad r=0. \quad (4c)$$

Equation 4b is derived from a mass balance on a control surface at $r = R$. Details are given in Appendix A.

Mass Balance for the Solid Phase. The mass-balance equation for the adsorbed solutes is derived from a shell balance within a particle as follows:

$$\frac{\partial q_i}{\partial t} = D_{si}\frac{1}{r^2}\frac{\partial}{\partial r}\left[r^2\frac{\partial q_i}{\partial r}\right] + y_{li}. \quad (5)$$

Here D_s is the surface diffusion coefficient, and q_i is the adsorbate concentration based on per solid sorbent volume. The D_s, defined in Eq. 5, is proportional to the intrinsic surface diffusion coefficient defined on the basis of concentration gradient per surface area. The D_s defined here and the D_s based on per surface area are related by a tortuosity factor for surface transport (Komiyama and Smith, 1974).

The initial condition is

$$q_i = q_i(t, r) \qquad t=0 \quad r \in [0, R], \quad (6)$$

and two boundary conditions are proposed below:

$$\frac{\partial q_i}{\partial r} = 0 \qquad r=0 \quad t \in [0, \infty] \quad (7a)$$

$$\frac{\partial q_i}{\partial t} = y_{li} + \frac{2D_{si}}{R}\frac{\partial q_i}{\partial r} \qquad r=R \quad t \in [0, \infty]. \quad (7b)$$

The boundary condition, Eq. 7b, is derived from mass balance; it states that the rate of change of q_i at $r = R$ is a result of net adsorption and surface diffusion. Detailed derivation of this equation is given in Appendix A.

Notice that Eq. 7b is different from those reported in the literature. Aris (1983) and Riekert (1985) proposed that the solid phase concentration gradient be set to zero at $r = R$.

$$\left.\frac{\partial q}{\partial r}\right|_{r=R} = 0.$$

This condition is equivalent to assuming only pore diffusion at the particle boundary. It is inappropriate for a general parallel diffusion model, because in the case of surface diffusion only, that is, $D_p = 0$, the $D_p(\partial c_p/\partial r)|_{r=R}$ term in Eq. 4b vanishes, resulting in no mass transfer into the particles, thus, no adsorption within the particle. Therefore, this boundary condition cannot be used for the general model proposed in this study.

Do and Rice (1987) assumed that the rate of change in q at $r = R$ is only balanced by adsorption, that is $(\partial q/\partial t)|_{r=R} = y_l$ is proposed as a boundary condition. This condition, however, implies that change in q at $r = R$ is purely due to net adsorption. It is inconsistent with Eq. 4b, which states that the flux due to film diffusion is balanced by the fluxes of both surface and pore diffusion at $r = R$. Equation 7b, on the other hand, does not have these drawbacks; it can be applied for the cases of pore diffusion alone, surface diffusion alone, or parallel pore and surface diffusion. More detailed derivation and discussion of the two key boundary conditions, Eqs. 4b and 7b, are given in Appendix A.

Adsorption Kinetics. For nonequilibrium adsorption in a multicomponent system, a generalized Langmuir kinetic equation has been proposed by Jin et al. (1994):

$$y_{li} = q_{si}(k_{ai}c_{pi}\phi_i - k_{di}\theta_i), \tag{8a}$$

where $\theta_i = q_i/q_{si}$, and ϕ_i is the surface availability function, which takes into account both steric hindrance and the competition between adsorbates; ϕ_i is a function of the surface coverages of all competing solutes. In the case of Langmuir kinetics $\phi_i = 1 - \sum_{i=1}^{N} \theta_i$. In general ϕ is a complex function of the individual coverages and the relative sizes of all solutes. When the finite sizes of hard disc adsorbates are considered, the availability function based on the scaled particle theory (SPT) has been proposed previously (Talbot et al., 1994):

$$\phi_i = \left(1 - \sum_{j=1}^{N} \theta_i\right) \exp\left[-\frac{\sum_{j=1}^{N} \theta_i\sigma_{ij}^2 + 2\sum_{j=1}^{N} \theta_i\sigma_{ij}}{1-\sum_{j=1}^{N} \theta_i} - \left(\frac{\sum_{j=1}^{N} \theta_i\sigma_{ij}}{1-\sum_{j=1}^{N} \theta_i}\right)^2\right], \tag{8b}$$

where q_{si} is the saturation capacity for the ith adsorbate, σ_{ij} is the ratio of the effective diameter of component i to that of component j. We note that, in the limit of equilibrium, $y_l = 0$, Eqs. 8a and 8b reduce to a set of isotherm equations.

$$c_{pi} = \frac{k_{di}\theta_i}{k_{ai}\phi_i}. \tag{8c}$$

For single-component systems, Eq. 8c resembles the Fowler–Guggenheim isotherm equation (Fowler and Guggenheim, 1960); they are equivalent at low surface coverage. The SPT model has been successfully used to correlate data for hydrophobic adsorption of small molecules in gas and liquid systems, and the kinetic equation of this model has been used to predict the breakthroughs of lysozyme in an affinity column at different feed concentrations; at high coverage, significant improvement is obtained compared to what the Langmuir kinetic equation predicted. More importantly, correlated sorbent capacities are in close agreement with those calculated from molecule sizes and sorbent surface areas (Jin et al., 1994). Therefore, Eq. 8c is used to correlate adsorption equilibrium data of two organic solutes in this study.

Mass Action Constant. For ion exchange systems, the following mass action constants are usually used in correlating multicomponent equilibrium data:

$$K_{d_{ij}} = \left(\frac{q_i}{c_{pi}}\right)^{Z_j}\left(\frac{c_{pj}}{q_j}\right)^{Z_i}, \tag{9a}$$

where q_i and q_j are the concentrations of ion i and j on the solid surface respectively; c_{pi} and c_{pj} are the corresponding concentrations in the liquid phase; and Z_i and Z_j are the valence of ion i and j, respectively. The detailed algorithm for solving q_i in a multicomponent system as a function of c_j according to Eq. 9a can be found in Klein (1984). Implementation of the mass action equation in VERSE-LC, a simulation package for multicomponent chromatography (Berninger et al., 1991), has been reported elsewhere (Ernest, 1994).

When the adsorption kinetics are slow, the following mass action kinetic equations are used:

$$y_{l_{ij}} = \frac{1}{q_{si}}\left(k_{a_{ij}}c_{pl}^{Z_j}q_j^{Z_i} - k_{d_{ij}}q_i^{Z_j}c_{pj}^{Z_i}\right). \tag{9b}$$

Notice that when in equilibrium, Eq. 9b reduces to the equilibrium isotherm shown in Eq. 9a.

Generalized Model in Dimensionless Variables. To simplify the equations discussed, we defined the dimensionless variables and rewrote the model equations in Appendix B.

The equations in Appendix B are the complete set in dimensionless form for the generalized model. We note that for multicomponent systems, only the convection rate is independent of solute properties; therefore, other transport rates are normalized by the convection rate.

The general model can be used for both nonequilibrium and equilibrium adsorption where all the mass-transfer processes are controlling. For specific cases, the actual values of the parameters defined in Eqs. B1 to B3 have to be determined and can be used for establishing model selection criterion. Table 2 summarizes the conditions for model selection.

There are mainly three quantities that determine the model selections: (N_p/KN_s), (Φ_k/N_p) and (Φ_k/KN_s). Pore diffusion

Table 2. Model Selection for Systems with Surface and Pore Diffusion*

Adsorption Kinetics	Appropriate Models		
	Pore	Surface	Parallel
Local equilibrium	$\Phi_k/N_p \gg 1$	$\Phi_k/(KN_s) \gg 1$	$\min\left(\frac{\Phi_k}{N_p}, \frac{\Phi_k}{KN_s}\right) \gg 1$
	$N_p/KN_s \gg 1$	$N_p/KN_s \ll 1$	$N_p/KN_s \cong 1$
Nonequilibrium	$\Phi_k/N_p \ll 1$	$\Phi_k/(KN_s) \ll 1$	$\max\left(\frac{\Phi_k}{N_p}, \frac{\Phi_k}{KN_s}\right) \ll 1$
	$N_p/KN_s \gg 1$	$N_p/KN_s \ll 1$	$N_p/KN_s \cong 1$

*Subscript i is omitted.

is the dominant mechanism when $N_p \gg KN_s$ (i.e., $D_p \gg D_s q_s k_a/k_d$), or surface diffusion dominates when $N_p \ll KN_s$ ($D_p \ll D_s q_s k_a/k_d$). Local equilibrium can be assumed when $\Phi_k \gg \max(N_p, KN_s)$. More importantly, in the case of parallel diffusion, especially when $N_p/KN_s \cong 1$, equilibrium can be assumed only when $\Phi_k \gg 1$ despite the fact that individual ratios (Φ_k/N_p) and (Φ_k/KN_s) can be quite large. It is worth emphasizing that when K is large, that is, the affinity of a solute or the capacity of the sorbent is high, the parallel diffusion model is needed, because surface diffusion may dominate at low concentration, whereas pore diffusion may dominate at high concentration, as shown in the "Results and Discussion" section.

In parallel transport systems, if pore diffusion mechanism is assumed in interpreting experimental data, although the intrinsic pore and surface diffusivities may very well be constant, one can obtain a concentration-dependent apparent pore diffusion coefficient; the higher the concentration, the smaller the apparent pore diffusion coefficient. On the other hand, if surface diffusion mechanism is assumed, a concentration-dependent apparent surface diffusion coefficient results; the higher the concentration, the higher the apparent surface diffusion coefficient. This is explained below.

For a single-component system, in the case of local equilibrium ($\Phi_k \gg 1$) and when both pore and surface diffusion are important, the following apparent pore diffusion coefficient can be derived from the generalized model:

$$D_{p_{app}} = D_p + \frac{1-\epsilon_p}{\epsilon_p} D_s \frac{\partial q}{\partial c_p}. \tag{10a}$$

Notice that this apparent pore diffusion coefficient strongly depends on the shape of the adsorption isotherm (Brecher et al., 1967; Aris, 1983; Riekert, 1985; Suzuki, 1982; Yoshida et al., 1994) as shown in Figure 1 for three typical isotherms. At infinitesimal concentration, the isotherm is linear, the apparent pore diffusion coefficient is a constant; therefore, parallel diffusion data can be analyzed by a pore diffusion model with a constant parallel pore diffusion coefficient, $D_{p_{app}}$, which, however, can be greater than the Brownian diffusivity if the K in Eq. B2 is sufficiently large. When the concentration is high enough to reach the nonlinear portion of the adsorption isotherm, the apparent pore diffusion coefficient becomes a function of the solute concentration; for the Langmuir isotherm, the apparent pore diffusion coefficient decreases

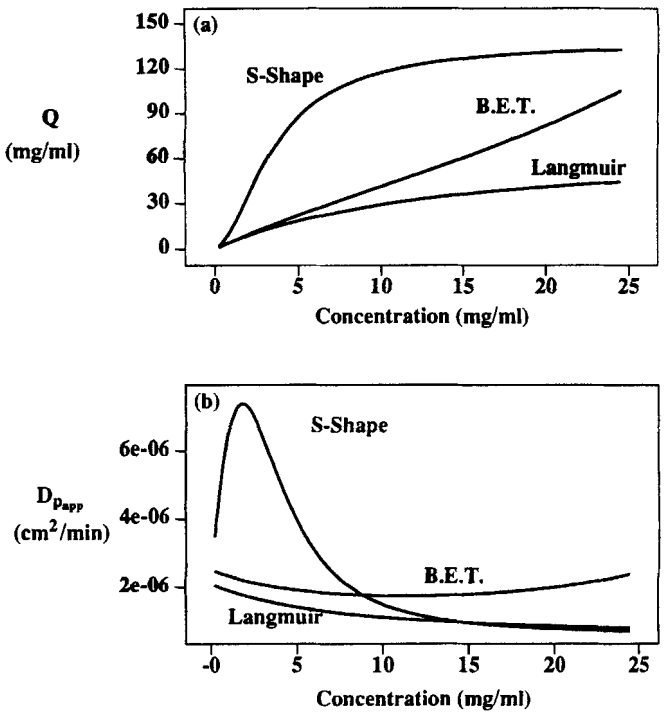

Figure 1. Dependence of the apparent pore diffusion coefficient on the shape of the isotherms.

Langmuir Equation: $q = \frac{q_s K_1 c_p}{1 + K_1 c_p}$ where $A = q_s K_1$, $B = K_1$.

BET Equation: $q = \frac{q_s \beta c_p / c_p^0}{(1 - c_p/c_p^0)[1 + (\beta - 1)c_p/c_p^0]}$.

S-Shape Equation: $q = \frac{q_s c_p (K_1 + 2K_2 c_p)}{1 + K_1 c_p + K_2 c_p^2}$

where $q_s = 69.19$, $K_1 = 0.073$, $K_2 = K_1/4$, $\beta = 50K_1$.

with increasing concentration. Therefore, when the solute affinity is high, the intraparticle diffusion cannot be described by a constant apparent pore diffusion model. Furthermore, even if the surface diffusion coefficient is small, the surface diffusional flux can still be large compared to that of pore diffusion, because of a large surface concentration gradient.

If one considers only surface diffusion and lumps pore diffusion into surface diffusion, an analogous apparent surface diffusion coefficient can be derived,

$$D_{s_{app}} = D_s + \frac{\epsilon_p}{1-\epsilon_p} D_p \frac{\partial c_p}{\partial q}. \tag{10b}$$

One can see that $D_{s_{app}}$ is concentration dependent and increases with increasing concentration for a Langmuir-type isotherm.

In multicomponent chromatography, in the mixing region where solute bands are partially separated, more than one solute is present. Both the apparent pore and surface diffusion coefficient are complex, highly nonlinear functions of all the solute concentrations. The partial derivative ($\partial q_i/\partial c_{pi}$) may not be monotonic. Even for the Langmuir isotherm, strongly nonlinear dependence of the apparent diffusion co-

efficient on solute concentration can result. To model such processes, the parallel diffusion model has to be used in addition to accurate information on adsorption kinetics and equilibria.

Method of numerical analysis

The set of proposed equations are solved using the orthogonal collocation on finite element (OCFE) method (Villadsen and Michelsen, 1978). In solving the equations, we discretized the z-axis to N_A elements; on each element orthogonal polynomials are used for each component to interpolate the concentration profiles; in between two adjacent elements, continuity conditions are enforced. The whole particle is treated as one element and an orthogonal polynomial is used to interpolate the concentration profiles in both the pore and the solid phase. The algorithm and the integration routine used are the same as in Berninger et al. (1991).

Any numerical method can introduce errors in a solution. Some of the errors cause extra dispersion on concentration waves that is not due to physical mechanisms (Lin et al., 1989). Such numerical dispersion introduced by a finite-difference scheme has been used to approximate the physical dispersion, by choosing discretization and integration step sizes according to the Courant condition (Courant and Friedrichs, 1948), which relates the step sizes to the solute distribution factor and the linear velocity (Lin et al., 1989). However, this approach is viable only in the case of a single-component system (Lin et al., 1989). For a multicomponent system, the dispersion for each solute is different; therefore, a different step size has to be used for each component, and it is impossible to implement such an algorithm.

Accuracy of an algorithm is crucial to the studies of diffusion-controlled processes. The first-order information, such as breakthrough time, or the retention time for a pulse, can be easily obtained from a finite-difference solution. By contrast, the second-order information, such as dispersion on elution peaks or breakthroughs, requires higher than second-order accuracy of the numerical algorithm. It is shown that OCFE is of such high accuracy (Baker, 1983) and gives a more accurate account for the dispersion than typical finite-difference schemes (Ma and Guiochon, 1991). This is the key reason that OCFE was used in this study.

In order to ensure convergence in our numerical solutions, all the simulation parameters are tested, including (1) number of axial elements (N_A); (2) number of axial collocation points (N_{Ac}); (3) number of collocation points in the sorbent particle (N_{Ap}); (4) absolute tolerance (A_{bs}); (5) relative tolerance (R_t); and (6) integration time step (Δt). A numerical solution is considered converged in this study when increases in N_A, N_{Ac}, N_{Ap} and decreases in A_{bs}, R_t, and Δt do not cause any change in the solution. In addition, we also benchmarked the converged solutions against two analytical solutions obtained from moment analysis (see next section) to ensure that the numerical solutions are free of other errors. In this study, sufficient accuracy is obtained using the following simulation parameters: $N_A = 50$–100; $N_{Ac} = 2$–4; $N_{Ap} = 2$–6; $A_{bs} = 0.001 c_f$; $R_t = 0.1\%$; $\Delta t = 0.01$ bed volume.

Equations for transport and adsorption shown in this work, as well as the isotherms and kinetic equations that are different from those reported previously (Berninger et al., 1991), have been integrated into the simulation package VERSE-LC. This package now takes into account axial dispersion, film mass-transfer resistance, parallel pore and surface diffusion, local equilibrium and nonequilibrium adsorption, as well as reactions in both liquid and solid phase. This study is mainly focused on the local equilibrium cases without any reactions. Studies on nonequilibrium adsorption here are limited to comparison of numerical solutions with an analytical solution. Detailed studies on the effects of nonequilibrium adsorption using the pore diffusion model can be found elsewhere (Whitley et al., 1993; Jin et al., 1994). For the simulation of local equilibrium cases reported below, the parameters k_a and k_d are chosen to be sufficiently large so that Φ_k is much greater than unity and always much greater than N_p or KN_s. The ratio of k_a/k_d, of course, should be equal to that of the equilibrium constant.

Analytical solutions obtained from moment analysis for locally linearized kinetics or isotherms

In chromatography simulations, when solute bands are partially separated, competition effects are strongest in the mixing zone where concentrations change significantly. It is in such regions that numerical dispersion has its strongest effect on the elution profiles (Ma et al., 1991). Although converged solutions can be obtained, large discrepancies are found in the interference zones calculated based on finite-difference schemes as a result of numerical dispersion (Lin et al., 1989), which depends in part on local solute concentrations. In order to simulate such competition effects accurately, the dispersion at different solute concentrations has to be understood. One way is to benchmark numerical solutions against analytical solutions, but there is no analytical solution available at present for the set of equations (Eqs. 1 to 7). Kucera (1965), Kubin (1965), Schneider and Smith (1968a) have reported moment analysis solutions for systems similar to those formulated in this work. Yet their solution is valid only when the isotherm is linear, or when the solute concentrations are infinitely small; therefore, it cannot be used for benchmarking numerical solutions at finite concentrations. In the following, we extend their solutions for two cases—equilibrium parallel pore and surface diffusion, and nonequilibrium pore diffusion—to pulse on plateau input conditions. The second-order central moment is then obtained at finite concentrations for these two cases, such that the dependence of dispersion on solute concentration can be analyzed. The main goal here is to use the analytical solutions as benchmarks for the numerical solutions so that accuracy and convergence of the numerical algorithm, as well as accuracy of the software coding, can be assured.

Equilibrium Parallel Pore and Surface Diffusion System. In a single-component system, if the bed is preequilibrated with C_b^0, C_p^0, and θ^0 followed by a small pulse perturbation, the appropriate mass-balance equation will have the following form:

$$\left(1 + K \left.\frac{\partial \theta}{\partial C_p}\right|_{C_p^0}\right) \frac{\partial \Delta C_p}{\partial \tau} = \left(N_p + KN_s \left.\frac{\partial \theta}{\partial C_p}\right|_{C_p^0}\right) \nabla_s^2 \Delta C_p, \quad (11)$$

where $\Delta C_p = C_p - C_p^0$, $\Delta\theta = \theta - \theta^0$. Note $C_p^0 = C_b^0$, which is the feed concentration used to preequilibrate the column, and

all the derivatives are zero at C_p^0, θ^0; only the equations pertaining to the perturbation are relevant here.

In this case, when the perturbations are small, solving Eq. 11 for the first-order and second-order central moment with an impulse input (Kubin, 1965; Schneider and Smith, 1968a), we have

$$\tau_r = \frac{\tau_p}{2} + \left(1 + \frac{2}{Pe}\right)\left[1 + \frac{1-\epsilon_b}{\epsilon_b}\epsilon_p\left(1 + K\frac{\partial\theta}{\partial C_p}\bigg|_{C_p^0}\right)\right], \quad (12)$$

where τ_p is the pulse width and τ_r is the first-order moment, for example, the retention time of the mass center of a peak. When $Pe \gg 2$, the preceding equation reduces to

$$\tau_r = \frac{\tau_p}{2} + \left[1 + \frac{1-\epsilon_b}{\epsilon_b}\epsilon_p\left(1 + K\frac{\partial\theta}{\partial C_p}\bigg|_{C_p^0}\right)\right]. \quad (13)$$

The solution for the second-order central moment is

$$\sigma_\tau^2 = 2\left[\left(1 + \frac{2}{Pe}\right)\delta_1 + \left(\frac{1}{Pe} + \frac{4}{Pe^2}\right)(1+\delta_0)^2\right] + \frac{\tau_p^2}{12} \quad (14)$$

where,

$$\delta_0 = \frac{1-\epsilon_b}{\epsilon_b}\epsilon_p\left(1 + K\frac{\partial\theta}{\partial C_p}\bigg|_{C_p^0}\right) \quad (15a)$$

$$\delta_1 = \frac{(1-\epsilon_b)\epsilon_p}{15\epsilon_b}\left(1 + K\frac{\partial\theta}{\partial C_p}\bigg|_{C_p^0}\right)^2\left(\frac{1}{N_{p_{app}}} + \frac{5}{B_f}\right). \quad (15b)$$

When $Pe \gg 4$, Eq. 14 reduces to

$$\sigma_\tau^2 = 2\left[\delta_1 + \frac{1}{Pe}(1+\delta_0)^2\right] + \frac{\tau_p^2}{12}. \quad (16)$$

Note when $C_p^0 \to 0$, Eqs. 15a and 15b are of the same form as for a linear isotherm.

Nonequilibrium Pore Diffusion Systems. The first-order and the second-order central moment can be derived by solving the perturbed form of Eqs. B5 and B6 together with the linearized kinetic equation shown in Appendix C (Eq. C10). The first-order moment for the nonequilibrium system is the same as for the equilibrium system, Eq. 13. The second-order central moment is

$$\sigma_\tau^2 = 2\left[\delta_1 + \delta_k + \frac{1}{Pe}(1+\delta_0)^2\right] + \frac{\tau_p^2}{12}, \quad (17)$$

where

$$\delta_0 = \frac{1-\epsilon_b}{\epsilon_b}\epsilon_p\left(1 + K\frac{\partial\theta}{\partial C_p}\bigg|_{C_p^0,\,\theta^0}\right) \quad (18a)$$

$$\delta_1 = \frac{(1-\epsilon_b)\epsilon_p}{15\epsilon_b}\left(1 + K\frac{\partial\theta}{\partial C_p}\bigg|_{C_p^0,\theta^0}\right)^2\left(\frac{1}{N_p} + \frac{5}{B_f}\right) \quad (18b)$$

$$\delta_k = \frac{(1-\epsilon_b)\epsilon_p}{\epsilon_b}\left(K\frac{\partial\theta}{\partial C_p}\right)^2\frac{C_p^0}{\theta^0}\frac{1}{\Phi_k}. \quad (18c)$$

Equations 16 and 17 are the solutions for the second-order central moment for a pulse on a plateau input condition. One can see that, when $\Phi_k \gg 1$, Eq. 17 reduces to Eq. 16, the solution corresponding to the equilibrium case. Note here the pore phase concentration C_p^0 is equal to the bulk interstitial phase concentration C_b^0.

Usually in chromatography, the efficiency of a column is measured by the height of an equivalent theoretical plate (HETP) (Van Deemter et al., 1956), which is defined as

$$\text{HETP} = \left(\frac{\sigma_\tau}{\tau_r}\right)^2 L. \quad (19)$$

In this work, Eq. 19 is used as a benchmark for the HETP obtained from numerical solutions as discussed next.

Calculation of HETP from Numerical Solutions. The first-order moment is defined as (Suzuki, 1973; Kubin, 1965; Kucera, 1965)

$$\tau_r = \frac{\int_{-\infty}^{+\infty}\tau C_b\, d\tau}{\int_{-\infty}^{+\infty} C_b\, d\tau}, \quad (20)$$

and the second-order central moment is defined as

$$\sigma_\tau^2 = \frac{\int_{-\infty}^{+\infty}(\tau-\tau_r)^2 C_b\, d\tau}{\int_{-\infty}^{+\infty} C_b\, d\tau} \quad (21)$$

Numerical solutions of column effluent histories are given concentrations as a function of time. To derive the first- and the second-order central moment defined earlier, a numerical integration routine in FORTRAN is written, and the HETP is calculated using Eqs. 19, 20 and 21. Note the integration in the denominator in Eqs. 20 and 21 is the peak area, which can be used to check the accuracy of the integration algorithm. Also the integrated area depends on the number of points obtained from the numerical solution routine. In this study, the simulation parameters used are such that the calculated area from the numerical solution is within 3% of what was injected and sufficient accuracy is achieved as shown in the results.

Results and Discussion

HETP values are obtained from numerical solutions and are benchmarked against those from the moment analysis. Parametric studies for single and binary systems are discussed next. Finally, calculated breakthroughs are compared with experimental data for adsorption of two organic solutes and ion exchange of strontium.

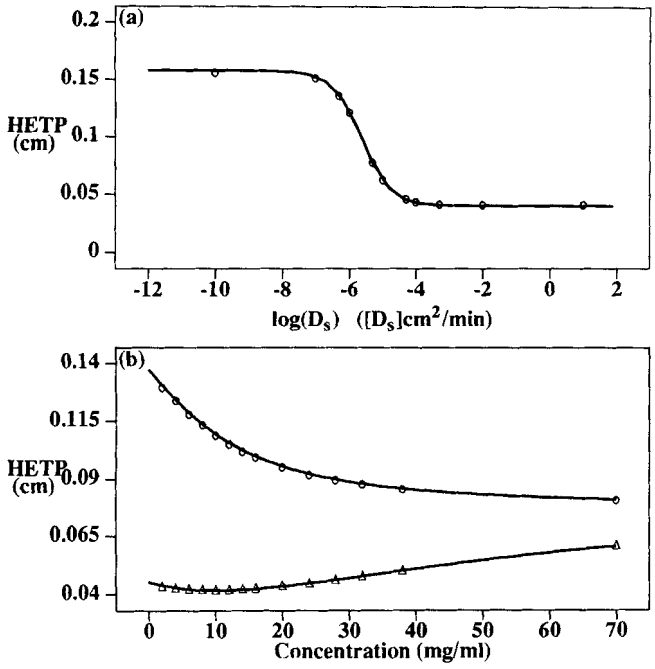

Figure 2. Dependence of HETP on: (a) surface diffusion coefficient and (b) loading concentration.

Line: calculated from Eqs. 16 and 19. Symbols: obtained from simulation with: (a) an impulse input condition; (b) a pulse on a plateau input condition. Circles: $D_s = 5 \times 10^{-7}$ cm^2/min. Triangles: $D_s = 5 \times 10^{-5}$ cm^2/min. $D_p = 5 \times 10^{-6}$ cm^2/min. Additional simulation parameters are listed in Table 3.

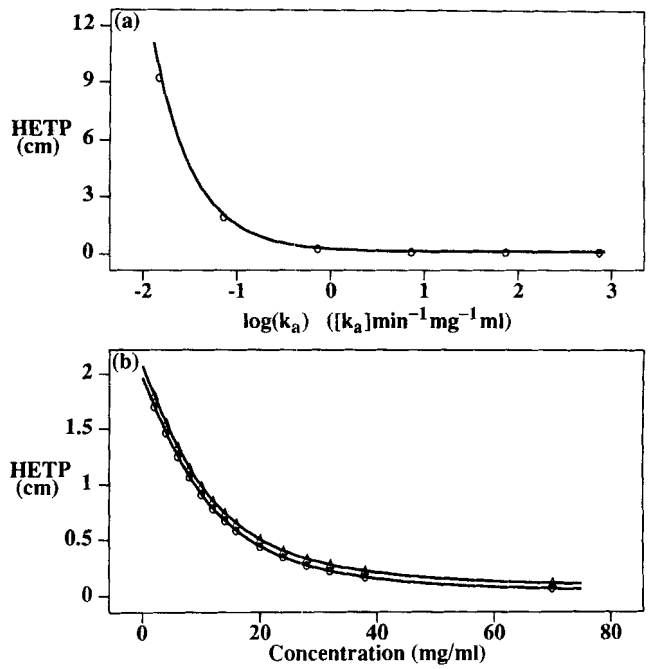

Figure 3. Dependence of HETP on: (a) adsorption rate constant and (b) feed concentration when adsorption kinetics is slow.

Simulation parameters are listed in Table 3. Line: from Eqs. 17 and 19. Symbols: from simulation with an impulse input condition using Eqs. 19, 20 and 21. $k_a = 0.0731$. Triangles: $D_p = 5 \times 10^{-6}$ cm^2/min. Circles: $D_p = 5 \times 10^{-5}$ cm^2/min.

Benchmark of numerical solutions

The benchmark results are shown in Figures 2 and 3. The parameters for numerical simulation are listed in Table 3. The HETP from the numerical solutions are calculated based on Eqs. 19, 20 and 21. Below we compare the HETP obtained from the numerical solutions with those from moment analysis over a wide range of pore diffusion coefficient, surface diffusion coefficient, solute affinity, and solute concentration.

Equilibrium Parallel Pore and Surface Diffusion. In Figure 2a, HETP vs. surface diffusion from the analytical solution are compared with those from simulation. In the simulation, a small pulse input is used. The surface diffusion coefficient is varied from 10^{-10} to 1 cm^2/min, while the pore diffusivity is kept constant. As shown in the figure, the calculated solution is in agreement with the analytical solution. We see that at the two extremes of the D_s values shown in the figure, HETP is controlled by D_p and k_f when D_s is small, whereas only HETP is controlled by k_f when D_s or D_p is large. This is implied by Eq. 15b, because when D_s is large, so is $N_{p_{app}}$, and $1/N_{p_{app}}$ in Eq. 15b vanishes.

At high concentration, HETP can be found from Eqs. 13, 15, 16, and 19 for a pulse on a plateau condition. Corresponding simulation is done using the pulse on a plateau input condition in VERSE. Figure 2b compares the HETPs calculated from simulations with those from the analytical solutions at different concentrations. Two cases are examined with different D_s values, while D_p is kept constant. The simulation results agree with those from the analytical solutions for both cases.

Nonequilibrium Pore Diffusion. Figure 3a shows the dependence of HETP on the adsorption rate constant k_a for a nonequilibrium pore diffusion case, where k_a values range from 0.07 to 800, which are selected to cover a wide range of

Table 3. System Parameters for HETP Simulation*

	L(cm)	ϵ_p	ϵ_b	ID (cm)	$R(\mu m)$	F_r(mL/min)
Column	25	0.702	0.391	0.45	10	0.5
Isotherm		Langmuir	A^*	B		
			5.061	0.07314		
Kinetic		q_s		k_a(mg·min/mL)$^{-1}$	k_d(min)$^{-1}$	
		69.19		7,314	10,000	
Mass transfer			E_b(cm^2/min)		k_f(cm/min)	
			3.124×10^{-2}		6.483×10^{-2}	

*The unit of the solid-phase concentration is per solid volume of stationary phase. $\tau_p \cong 0.025$.

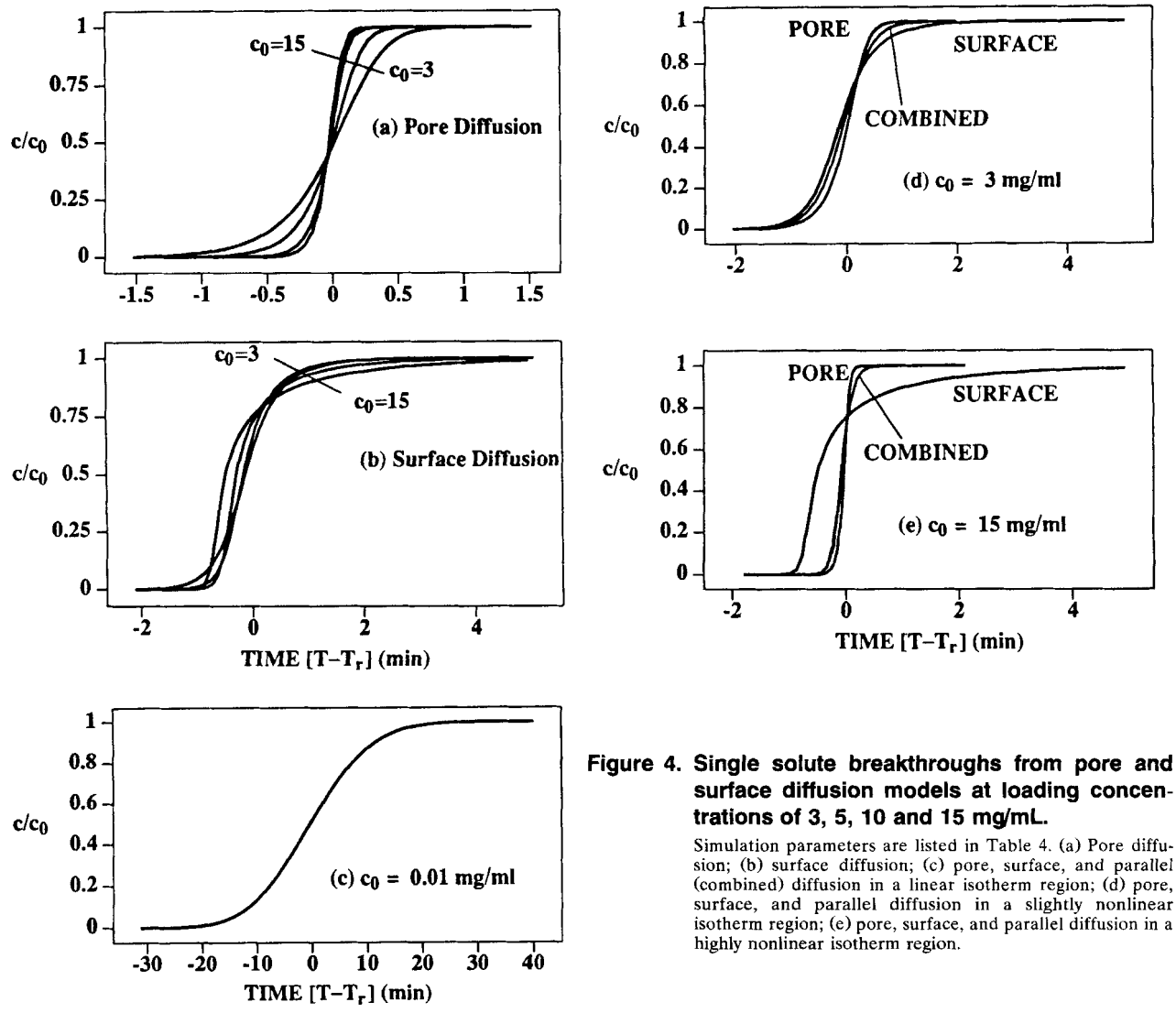

Figure 4. Single solute breakthroughs from pore and surface diffusion models at loading concentrations of 3, 5, 10 and 15 mg/mL.

Simulation parameters are listed in Table 4. (a) Pore diffusion; (b) surface diffusion; (c) pore, surface, and parallel (combined) diffusion in a linear isotherm region; (d) pore, surface, and parallel diffusion in a slightly nonlinear isotherm region; (e) pore, surface, and parallel diffusion in a highly nonlinear isotherm region.

analytical and preparative systems. The calculated HETPs agree with those from the analytical solution. Note when k_a is less than 1.0, split peak results (peaks are not shown here), in which case the HETP is not properly defined, yet the calculated values using Eqs. 19, 20 and 21 from the numerical solution agree very well with those of the analytical solution. Figure 3b shows the calculated HETPs at different loading concentrations under nonequilibrium conditions. Agreement between theoretical and simulation solutions is also achieved. Here, two cases with different pore diffusivities are examined. Change of the diffusivity by 10-fold does not have significant effect on the HETP, indicating that slow adsorption is controlling.

More benchmarks, which are not included here, have been done at different values of N_s, N_p, N_f, K, and Φ_k. Similar agreement has been achieved for all cases. This assures that the code is properly implemented and the numerical method is of sufficient accuracy.

In the following, we discuss the calculated breakthrough curves from single and binary systems. The simulation parameters used for these studies are based on a typical hydrophobic adsorption system. The purpose of the simulation is to show characteristic breakthrough behavior in a nonlinear isotherm system.

Effects of concentration and solute affinity on breakthrough curves of a single solute

In this section, single solute breakthroughs for a Langmuir isotherm case are examined with the parallel diffusion model. This isotherm is used because it is well known and mathematically simple.

Figure 4 compares the breakthrough predictions from the pore and the surface diffusion models in linear and nonlinear isotherm regions. *Note that the apparent pore diffusion coefficient at zero coverage is kept constant for all cases, meaning that in a linear isotherm region or at infinitesimal concentrations, breakthroughs predicted from the pore diffusion model are identical to those from the surface diffusion model.* Figure 4a shows that in pore diffusion as step change in concentration increases, breakthroughs become steeper, because pore diffusion flux increases and self-sharpening due to increasing

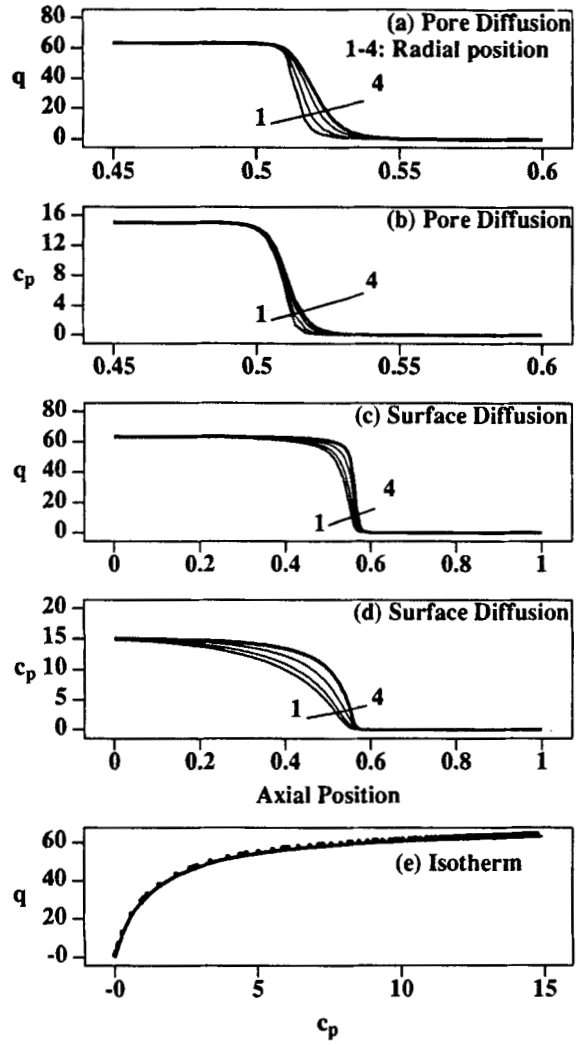

Figure 5. Column profiles for the cases in Figure 4 and q vs. c_p plot at four collocation points (1= inner, 4 = outer) at 6.5 min.

Simulation parameters are the same as those in Figure 4. (a) Solid-phase axial concentration profiles for pore diffusion; (b) pore phase axial concentration profile for pore diffusion; (c) solid phase axial concentration profiles for surface diffusion; (d) pore phase axial concentration profiles for surface diffusion; (e) q and c_p plot at all collocation points.

isotherm nonlinearity also increases. In the case of surface diffusion, although the breakthrough curves are sharpened in nonlinear isotherm regions (Figures 4d and 4e) compared to that in the linear isotherm region (Figure 4c), breakthroughs show more pronounced tailing with increasing step change in concentration (Figure 4b). This tailing is due to a finite adsorption capacity and is further explained in Figure 5.

Figure 4c compares the breakthroughs for surface diffusion, pore diffusion, and parallel diffusion at a low feed concentration, where the isotherm is linear and the apparent surface and pore diffusion coefficients are identical. As expected, the breakthroughs for all models are the same. In Figure 4d the feed concentration is in a slightly nonlinear isotherm region (see Figure 5e). The breakthrough curve from parallel diffusion is in between those of the pore and surface diffusion. However, when the concentration step spans a highly nonlinear isotherm region, as shown in Figure 4e, although the same apparent $D_{s_{app}}$ and $D_{p_{app}}$ are used for all three cases, the breakthrough curve from parallel diffusion shifts toward that of pore diffusion, indicating apparent dominance of pore diffusion over surface diffusion. Therefore, for high-affinity or high-capacity systems, the parallel model has to be used when the intrinsic D_s is nonzero, because the dominant intraparticle diffusion mechanisms at low and high concentrations are different; the breakthrough curves over a wide concentration range cannot be described by an effective pore diffusion coefficient or an effective surface diffusion coefficient using the single-diffusion models.

Note in the surface diffusion case that the breakthrough of high feed concentration is asymmetric and occurs earlier than that from pore diffusion. Such tailing and early breakthrough are caused by the slow diffusion on the surface compared to those in the pore phase; Figure 5 shows the column profiles at four different collocation points (along radial direction) at 6.5 min after the introduction of the solute. There are large differences between the profiles in Figures 5a and 5b and those shown in Figures 5c and 5d along the column axial direction. In the case of surface diffusion (Figures 5c and 5d), the apparent intraparticle diffusion coefficient is maximum when the surface is clean, resulting in a sharper change in the breakthrough concentration. When the breakthrough concentration reaches the nonlinear isotherm region, the surface concentration gradient reaches a limit because of limited surface adsorption capacity, resulting in an overall intraparticle diffusion flux that is lower than that of pore diffusion; this causes the early breakthrough and the pronounced tailing as shown in Figure 4b. In contrast, the concentration gradient for pore diffusion increases proportionally with increasing concentration; the self-sharpening effects are not impeded by any limitation of intraparticle diffusion. Therefore, the breakthroughs remain sharp and symmetric as shown in Figure 4a. In the simulation, solid- and liquid-phase concentrations were found, as expected, to follow the equilibrium isotherm at all collocation points (Figure 5e).

Tailing in a breakthrough curve can also be caused by a gradually decreasing adsorption rate due to steric blocking of the adsorbed molecules at high surface coverage in nonequilibrium adsorption. The slowing down of the adsorption rate also results in dispersed breakthroughs at high concentration (Jin et al., 1994). The slow approach to saturation caused by surface diffusion and by steric hindrance of adsorbates can be differentiated as follows; the steric blocking of the adsorbed molecules usually gives rise to a non-Langmuir isotherm and thus a nonlinear Scatchard plot. If the Scatchard plot is linear and breakthrough curves become more asymmetric and dispersed with increasing concentration, surface diffusion, instead of steric blocking, is likely the cause of tailing.

Effect of parallel diffusion on binary system breakthroughs

Figure 6 compares the breakthroughs from the pore and the surface diffusion model where the apparent diffusion coefficient of the high-affinity solute (H) is ten times of the low-affinity solute (L). Three cases are shown: pore diffusion, surface diffusion, and parallel diffusion. The apparent pore diffusion coefficients in all three cases are identical in linear isotherm regions. Figure 7 shows the same cases as in Figure

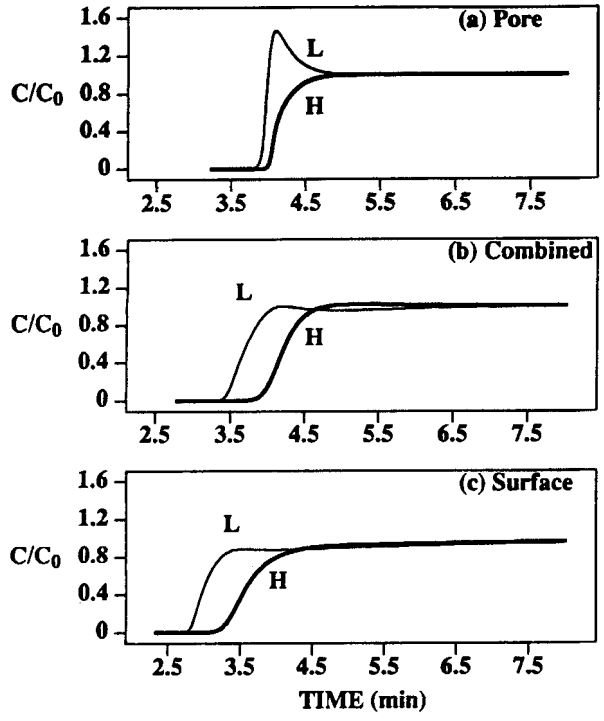

Figure 6. Binary breakthroughs from pore, parallel, and surface diffusion models.

The two solutes have different apparent diffusion coefficients. $D_{appH} = 10^{-5}$ cm^2/min $= 10 \times D_{appL}$. Other parameters are in Table 5.

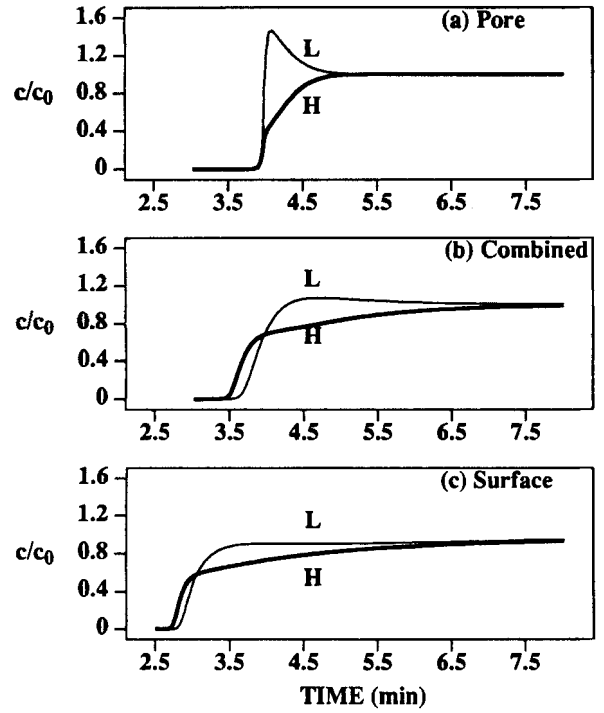

Figure 7. Comparison of binary breakthroughs from pore, surface, and parallel diffusion.

The two solutes have different apparent diffusion coefficients. $D_{appL} = 10^{-5}$ cm^2/min $= 10 \times D_{appH}$. Other parameters are the same as in Figure 6.

6 except the apparent pore diffusion coefficient of the less retained is now ten times of the more retained. We see that when the less retained species diffuses faster in the particle than the more retained solute, elution order change is predicted by the surface and the parallel diffusion model, but not predicted by the pore diffusion model. When two species have different intraparticle diffusion rates, separation occurs (defined as "kinetic separation"). When the apparent diffusion coefficient of the more retained species is ten times larger than the less retained species, the separation governed by adsorption isotherm is enhanced by kinetic separation (Figure 6). If the adsorption affinity of the fast-diffusing solute is less than that of the slow-diffusing solute, kinetic separation is against that determined by the equilibrium isotherms, causing the elution order reversal, as shown in Figure 7. In contrast, the pore diffusion model predicts that separations governed by the equilibrium isotherm are dominant because of the large concentration gradient in the liquid pore phase at high concentration. Figure 8 shows the column profiles, taken

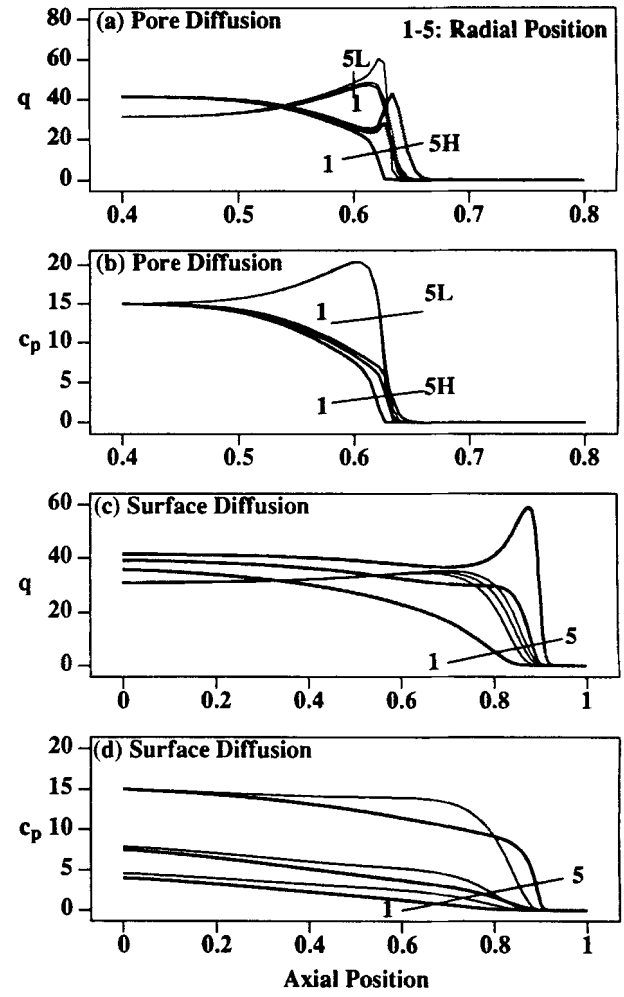

Figure 8. Axial column profiles at 2.5 min for the pore diffusion model in Figure 7.

Only the concentrations at three particle collocation points 1 (inner), 3, and 5 (near the particle surface) are shown. (a) Solid phase concentration for pore diffusion; (b) pore phase concentration for pore diffusion; (c) solid phase concentration for surface diffusion; (d) pore phase concentration for surface diffusion. Thick line: high affinity solute; thin line: low affinity solute.

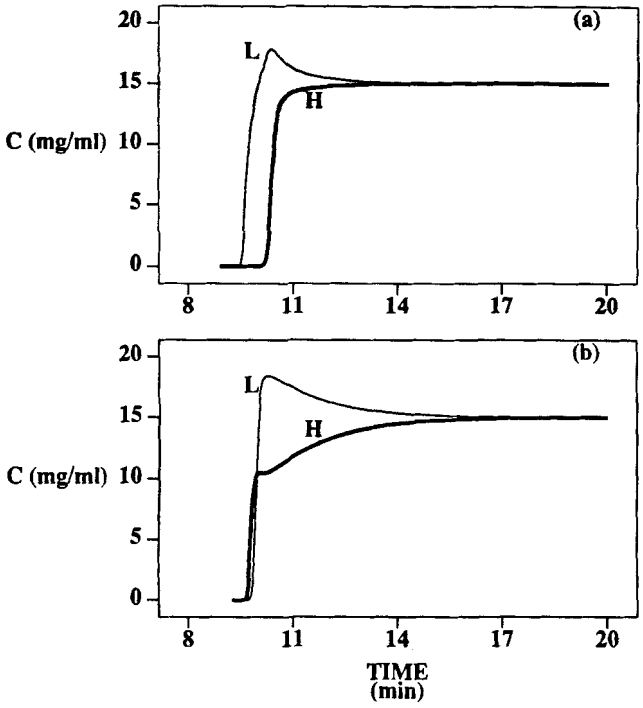

Figure 9. Binary breakthroughs from the pore and surface diffusion models.

The two solutes have different transport mechanisms. Other parameters are the same as in Figure 6. (a) $D_{pH} = 3.2838 \times 10^{-4}$ cm^2/min; $D_{sH} = 0$; $D_{pL} = 0$; $D_{sL} = 1.0419 \times 10^{-5}$ cm^2/min. (b) $D_{pL} = 2.4878 \times 10^{-4}$ cm^2/min; $D_{sL} = 0$; $D_{pH} = 0$; $D_{sH} = 1.0314 \times 10^{-5}$ cm^2/min.

2.5 minutes after the introduction of the solutes, for the pore diffusion and the surface diffusion cases of Figure 7. We see in Figure 8c and 8d that the surface diffusion model predicts the elution order governed by the isotherm in the interior collocation point (point 1), but at an outer collocation point the elution order is reversed (point 5). The high affinity solute band crosses the low affinity solute band at the middle point (point 3).

Figure 9 compares the breakthroughs when the diffusion mechanisms of two solutes are different; that is, one through pore diffusion, the other through surface diffusion. If pore diffusion is dominant for the more retained solute and surface diffusion is dominant for the less retained solute, separation is enhanced (Figure 9a). In contrast, if pore diffusion is dominant for the less retained solute and surface diffusion is dominant for the more retained solute, separation of the two fronts is impeded (Figure 9b); there is an elution order change similar to that shown in Figure 7c. Note that the apparent diffusion coefficients of the two components are kept identical in the two cases.

Comparison of simulation with experimental data

Adsorption of DMP and DCP on Activated Carbon. The experimental data for the adsorption of dimethylphenol (DMP) and dichlorophenol (DCP) on activated carbon were obtained from Thacker et al. (1984). In the original reference, many more breakthrough curves under different experimental conditions were reported. The original authors applied a surface diffusion model and a consistent set of equilibrium and mass-transfer parameters to explain the breakthrough curves. Only a typical case is analyzed in this study and presented below. The original studies used an equilibrium adsorption model without considering axial dispersion or pore diffusion. In the current work, all these effects are included, and a generalized parallel diffusion model for both equilibrium and nonequilibrium adsorption is developed. Because of these fundamental differences, mass-balance equations as well as boundary conditions are different from those in the original reference.

In the experiment shown below, the solutions contained 0.05-M phosphate buffer to maintain the pH at 6, at which the neutral forms of the two phenolic species were dominant. The equilibrium data were obtained from batch equilibration tests and the equilibrium liquid and solid phase concentrations were given in Table 3 of Thacker et al. (1984). Detailed descriptions of the experiments are given in the original reference. The equilibrium and kinetic parameters and the experimental system parameters used in the simulation are listed in Table 6.

Figure 10 shows the adsorption equilibrium data for DMP and DCP and the comparison between the data and predictions from different isotherm models. The SYSNLIN, a procedure in SAS that treats multiobjective and multivariant systems, is used for the correlation. Note that three isotherm models are used in correlating the experimental data: the modified ideal adsorbed solution (IAS) model (Thacker et al., 1984), the SPT (Eq. 8c), and the Langmuir model. Figure 10a and 10b compare the modified Freundlich correlations from the original reference and the SPT for single-component isotherms. Figure 10c and 10d compare the binary data with the predictions from Langmuir, modified IAS, and SPT (the data and the modified IAS predictions were from Table 3 in

Table 4. System Parameters for Single Component Simulation

Column	L (cm)	ϵ_p	ϵ_b	ID (cm)	R (μm)	F_r (mL/min)
	25	0.702	0.391	0.45	50	0.5
Isotherm			A**	B		
			5.061	0.07314		
Kinetic	q_s			k_a (mg·min/mL)$^{-1}$	k_d (min)$^{-1}$	
	69.19			7,314	10,000	
Mass transfer	D_p^*(cm^2/min)		D_s^*(cm^2/min)	E_b(cm^2/min)	k_f(cm/min)	
	5.0×10^{-5}		1.0×10^{-5}	3.124×10^{-2}	6.483×10^{-2}	
Dimensionless	Φ_k	N_p	N_s	N_f	K	
	6.680×10^5	6.219	1.244	1.884×10^2	2.1482	

*The values shown here are the intrinsic pore and surface diffusion values.
**The unit of the solid-phase concentration is per solid volume of stationary phase.

Table 5. System Parameters for Two Component Simulations

Column	L (cm)	ϵ_p	ϵ_b	ID (cm)	R (μm)	F_r (mL/min)
	10	0.702	0.391	0.45	25	0.5
Isotherm		A_1	B_1		A_2	B_2
		56.25	0.75		75.00	1.00
Kinetic		q_s	k_a (mg·min/mL)$^{-1}$		k_d (min)$^{-1}$	
Solute 1		75	750		1,000	
Solute 2		75	1,000		1,000	
Mass Transfer	D_p^* (cm^2/min)		D_s^* (cm^2/min)			
Solute 1	1.0×10^{-5}		1.0×10^{-5}			
Solute 2	1.0×10^{-5}		1.0×10^{-5}			
Dimensionless	Φ_k	N_p	N_s		N_f	K
Solute 1	2.970×10^4	1.990	1.990		3.797×10^2	23.878
Solute 2	3.960×10^4	1.990	1.990		3.797×10^2	31.837

*The values shown here are the intrinsic pore and surface diffusion as in Eq. 10a. Other simulation parameters, which are not shown here, are the same as in Table 4 for both solutes.

Thacker et al., 1984). Note that the data points presented in Figure 10c are at different DCP concentrations, and the data points in Figure 10d are at different DMP concentrations. This results in nonsmooth prediction curves as shown in both figures. The predictions from SPT are not as good as those from the modified IAS, because there are only four fitted parameters in SPT, whereas there are eight fitted parameters in the modified IAS (Thacker et al., 1984). In spite of the differences in the isotherm correlations, sequential loading curves are well predicted by the SPT, as shown below.

The isotherm parameters obtained from fitting the batch equilibration data (Figure 10) are used in VERSE to simulate sequential loading. Other parameters, including D_s and k_f, are obtained from Thacker et al. (1984). Note in this example and the next, the large rate constants, k_a and k_d, are chosen so that local equilibrium is maintained.

Figure 11 compares the simulation results with the breakthrough curve. After the column is saturated with 0.990 mmole/L of DMP at $t = 1{,}202$ min, the adsorbed DMP is displaced by sequential loading of a mixture of 1.020 mmol/L of DCP (squares) and 0.990 mmol/L of DMP (circles). The simulation from surface diffusion (solid lines) and experimental data point (symbols) are shown in Figure 11a. Three simulation curves from the pore diffusion model using different pore diffusion coefficients are compared with the data in Figure 11b. Clearly, in a highly nonlinear isotherm region, the pore diffusion model cannot account for the shape of the sequential breakthrough curves; when D_p is small, a hump occurs in the breakthrough of DMP, while when D_p is large (larger than the Brownian diffusivity), the breakthrough becomes sharper and occurs later than the experimental data; in addition, the DMP peak displaced by DCP and the breakthrough of DCP are poorly fitted. On the other hand, good agreement is achieved using the surface diffusion model, indicating that surface diffusion is dominant. The initial sharp rise and the subsequent tailing in the breakthrough data show the characteristics of surface diffusion in nonlinear isotherm systems (Figure 4b). The dominance of surface diffusion can be attributed to the high solute affinities; the K in Eq. B2 is quite high, about 10^5. Because of the high affinities, very little DMP and DCP remain in the pore fluid to generate significant concentration gradients for pore diffusion. Moreover, activated carbon is known to have many small pores (Noll et al., 1992), which can hinder pore diffusion and result in small D_p values, making pore diffusion contributions negligible compared to those of surface diffusion.

Ion-Exchange of Strontium, Sodium, and Calcium in Zeolite. The experimental data were obtained from Mercer and Ames (1963). In their study, competitive isotherm data were obtained from batch equilibration tests, and were correlated by three mass action constants. Zeolite was prepared in sodium form with saturated sodium chloride solution; it was washed with water and packed in water before the feed containing 0.2N N_a^+, 0.07N S_r^{++}, and 0.02N C_a^{++} was introduced into

Table 6. Adsorption of DMP and DCP on Activated Carbon

Column	L (cm)	ϵ_p	ϵ_b	ID (cm)	R (μm)	F_r (mL/min)
	5.05	0.62	0.40	1.88	254	33.114
Isotherm	σ	q_s	K_1			
DMP	1	9.016	1.034×10^4			
DCP	0.931	10.407	1.341×10^4			
Kinetic	β	q_s	k_a (M·min)$^{-1}$	k_d (min)$^{-1}$		
DMP	1	9.016	1.034×10^6	100		
DCP	0.931	10.407	1.341×10^6	100		
Mass Transfer	D_p^* (cm^2/min)		D_s^* (cm^2/min)	E_b (cm^2/min)		k_f (cm/min)
DMP	3.500×10^{-4}		2.472×10^{-7}	2.973		0.287
DCP	4.000×10^{-4}		3.030×10^{-7}	2.973		0.287
Dimensionless	Φ_k	N_p	N_s	N_f	K	
DMP	2.080×10^6	9.186×10^{-2}	6.488×10^{-5}	8.610	5.715×10^4	
DCP	2.262×10^6	1.050×10^{-1}	7.952×10^{-5}	8.610	8.555×10^4	

*The values of the diffusion coefficient listed here are for single-diffusion models.

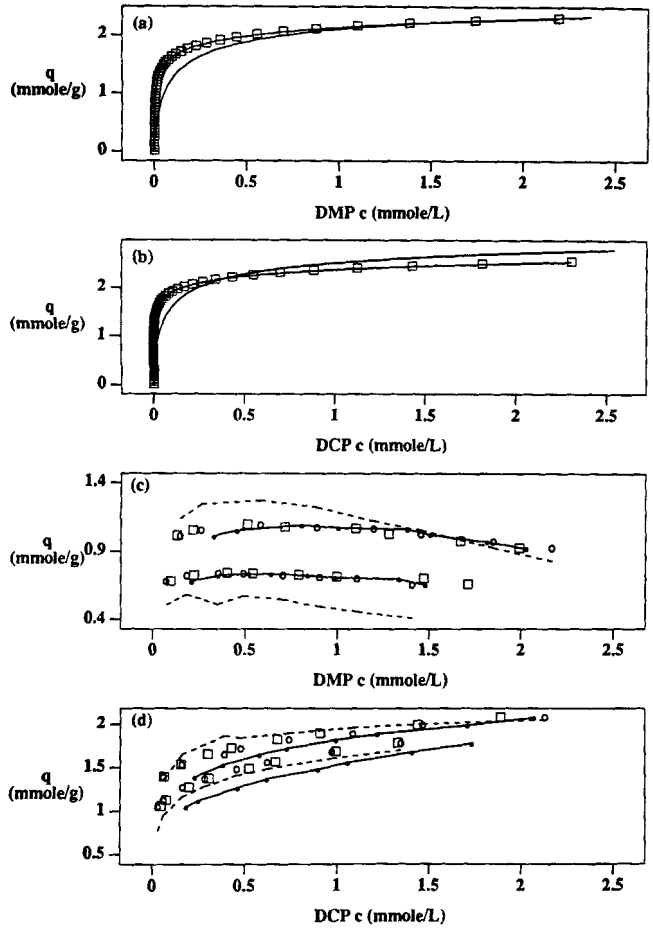

Figure 10. Single-component and binary and equilibrium adsorption data for DCP and DMP.

(a) DMP isotherm; solid line with symbols: three-parameter Freundlich isotherm; solid line only: SPT isotherm; (b) DCP isotherm; same convention as in Figure 10a; (c) and (d) solid line with dots: best fit from the equilibrium form of SPT equation. The parameters are listed in Table 6. Dashed line: best fit from the binary Langmuir equation. $A_1 = 26.111$; $A_2 = 86.387$; $K_1 = 8.925$, $K_2 = 35.652$. Squares: best fit from the modified IAS (Table 3, Thacker

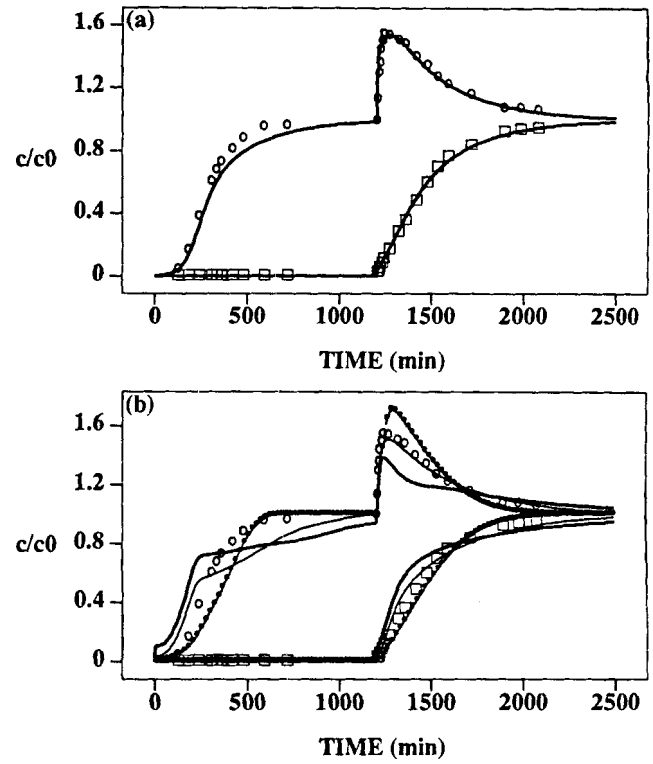

Figure 11. Simulation with experimental data for sequential adsorption of DMP (circles) and DCP (squares) on activated carbon.

Simulation parameters are listed in Table 6. (a) Thick solid lines: simulation from surface diffusion. (b) Simulation from pore diffusion. Thick lines: $D_{p_{DMP}} = 1.750 \times 10^{-4}$ cm^2/min; $D_{p_{DCP}} = 2.00 \times 10^{-4}$ cm^2/min. Thin lines: $D_{p_{DMP}} = 3.50 \times 10^{-4}$ cm^2/min; $D_{p_{DCP}} = 4.00 \times 10^{-4}$ cm^2/min. Lines with dots: $D_{p_{DMP}} = 1.25 \times 10^{-3}$ cm^2/min; $D_{p_{DCP}} = 1.35 \times 10^{-3}$ cm^2/min.

the column. The breakthrough experiments were performed at 80°C. Detailed descriptions of the experiments were given in the original reference.

The column and isotherm parameters for the simulation, listed in Table 7, are obtained from the original reference. The Brownian diffusivities of Sr^{++} at 80°C were reported by Mercer and Ames (1963). The Brownian diffusivities at 25°C for calcium and sodium are obtained from Cussler (1984) and corrected to 80°C using the Stokes–Einstein equation. Ideally, the pore diffusion coefficient of a solute should be obtained from the tortuosity factor of the sorbent and the Brownian diffusivity of the solute. The tortuosity factor can be determined from a pulse elution of a small nonadsorbing molecule (Miyabe et al., 1992). An apparent pore diffusion coefficient can be obtained from pulse-elution data using Eqs. 14 and 16. Then D_s can be estimated from Eq. 10a. However, in this case, neither pore nor surface diffusion coefficient is known from the original reference. The best fits are obtained by varying the pore and the surface diffusion coefficients, respectively, in the single-diffusion models, while keeping the tortuosity constant.

In a multicomponent system, the diffusion flux of a particular ion is influenced by the concentration gradient of all the ions present because an electrostatic potential develops during diffusion—the so-called Nernst–Planck diffusion effect (Helfferich, 1983). This coupled diffusion phenomenon is most pronounced at low ionic strength (< 1 mN) (Moynihan et al., 1988). The ion exchange system shown in Figure 12 has an ionic strength of 0.2N. The Nernst–Planck diffusion effect is expected to be insignificant for this system. Therefore, the use of Fick's law in the present model is justified.

Figure 12 compares the predictions from the pore and surface diffusion models with the experimental breakthrough curves of Sr^{++} for four different particle sizes. We see that the single diffusion model predictions look reasonable. However, a large apparent pore diffusion coefficient has to be used for the pore diffusion model, resulting in a tortuosity that is less than unity. This suggests that parallel diffusion is likely the intraparticle transport mechanism. It is also known from the literature that in micropores found in zeolites (Ruthven, 1984), surface diffusion is dominant, while pore diffusion is dominant in macropores, resulting in parallel transport (Robinson et al., 1994). For these reasons, we at-

Table 7. Ion Exchange for Sr^{++} System Parameters

Column	L (cm)	ϵ_p	ϵ_b	ID (cm)	R (μm)†	F_r (mL/min)
	21	0.32	0.40	1.9	550	11.9
Isotherm		q_s	K_d			
Sr^{++}		7.204	1.850			
Ca^{++}		7.204	0.420			
Na^{+}		7.204	1.00			
Kinetic		q_s	k_a (N·min)$^{-1}$	k_d (min^{-1})		
Sr^{++}		7.204	1.850×10^{4}	10^{4}		
Ca^{++}		7.204	0.420×10^{4}	10^{4}		
Na^{+}		7.204	1.000×10^{4}	10^{4}		
Mass Transfer	D_∞ (cm^2/min)	D_p^* (cm^2/min)		D_s^* (cm^2/min)	E_b (cm^2/min)	k_f (cm/min)
Sr^{++}	1.080×10^{-3}	5.750×10^{-4}		2.650×10^{-6}	2.188	2.022×10^{-1}
Ca^{++}	5.615×10^{-4}	2.989×10^{-4}		1.378×10^{-6}	2.188	1.168×10^{-1}
Na^{+}	9.453×10^{-4}	5.033×10^{-4}		2.319×10^{-6}	2.188	1.653×10^{-1}
Dimensionless	Φ_k	N_p	N_s	N_f	K	
Sr^{++}	5.664×10^{5}	0.380	1.752×10^{-3}	3.309×10^{1}	28.320	
Ca^{++}	5.664×10^{5}	0.198	9.111×10^{-4}	1.911×10^{1}	6.429	
Na^{+}	5.664×10^{5}	0.333	1.533×10^{-3}	2.705×10^{1}	15.308	

*Only the intrinsic pore and surface diffusion coefficients used in the parallel diffusion model are listed here.
†The largest particle size and the corresponding N_f, N_p, N_s, and Φ_k are listed here. E_b is obtained from the correlation reported by Chung and Wen (1968); k_f is obtained from the correlation reported by Wilson and Geankoplis (1966); and the D_p and D_s listed here are, respectively, the best fit values of the pore diffusion and the surface diffusion models.

tempted to explain the data using the parallel diffusion model. The thick solid lines in Figure 12 are predictions from the parallel diffusion model. In this case, the pore diffusion coefficient is 1.08×10^{-4} cm^2/min, which is estimated from the Brownian diffusivity (10.8×10^{-4}cm^3/min) reported in the original reference and a typical tortuosity factor of 3.3 for zeolites (Suzuki, 1990). The surface diffusion coefficient for Sr^{++} was estimated from best fitting of the four breakthroughs to be 2.65×10^{-6}cm^2/min. This estimated value is in the same order of magnitude as those reported in the literature for other zeolites (Robinson et al., 1994). Since Sr^{++} has a fairly high affinity for the zeolite, the apparent surface diffusion coefficient $D_{s_{app}}$ estimated from the surface diffusion model should be close to the intrinsic D_s. After subtracting the estimated D_p from $D_{s_{app}}$ according to Eq. 10b, a surface diffusion coefficient of 2.35×10^{-6}cm^2/min is obtained, and this value is used for the parallel diffusion simulation. One can see that reasonable predictions are obtained with the parallel diffusion model.

For the smallest particle case, the predictions from all three diffusion models deviate from the experimental data. This can be attributed to the following facts. In the experiments, zeolite pellets (1/16 in.) were crushed and sieved into four different mesh sizes, 16×18, 20×25, 30×35, and 45×50. It is possible that the distribution of macropores is substantially changed for the smallest (45×50 mesh) particles, and results in smaller pore diffusion coefficients. As shown in Figure 13, a 50% reduction in the pore diffusivities of all three ions gives a much closer prediction of the Sr^{++} breakthrough curve in Figure 12a. The misfit can also be due to nonideal packing of the small-particle column, which can cause a more dispersed breakthrough and an apparent uniform reduction of D_p for all solutes.

In the original reference there are no breakthrough data on sodium and calcium; therefore, only the simulation profiles are shown here. As indicated earlier, the bed was initially loaded with sodium. After the feed is introduced, sodium is displaced by calcium and strontium, causing the initial sodium concentration in the effluent to be higher than that in the feed. The calcium history displays a roll-up in the breakthrough curves as the high-affinity strontium displaces both calcium and sodium. In a parametric study (not shown here) when the diffusion coefficient of one solute changes, the breakthrough curves of the other two are greatly affected, indicating that intraparticle diffusion strongly affects competitive ion exchange in multicomponent systems.

Conclusions

A generalized model that incorporates both pore and surface diffusion for multicomponent adsorption and liquid chromatography has been formulated and solved numerically. Analytical solutions are obtained from moment analysis for locally linearized kinetics and equilibrium isotherm systems and used as benchmarks for numerical solutions. Agreement has been achieved over a wide range of concentration, affinity, pore diffusivity, and surface diffusivity. Model predictions are in close agreement with experimental data for two systems: ion-exchange of strontium in zeolite for nuclear waste treatment and adsorption of organics on activated carbon for waste water treatment.

Three ratios have been found to be critical to model selections: (N_p/KN_s), (Φ_k/N_p), and (Φ_k/KN_s). When $\Phi_k \gg 1$ and $\Phi_k \gg N_p$ or KN_s, local equilibrium is maintained. When $KN_s \gg N_p$, surface diffusion is dominant, whereas when $N_p \gg KN_s$, pore diffusion is dominant. When the solute affinities or the sorbent capacities are high, surface diffusion should be considered, even though the intrinsic surface diffusion coefficients are small.

Parametric studies of pore and surface diffusion for single-component and binary systems have been conducted. In linear isotherm systems, both pore and surface diffusion cause symmetric spreading of breakthrough curves. An effective pore or surface diffusivity can be used in the respective

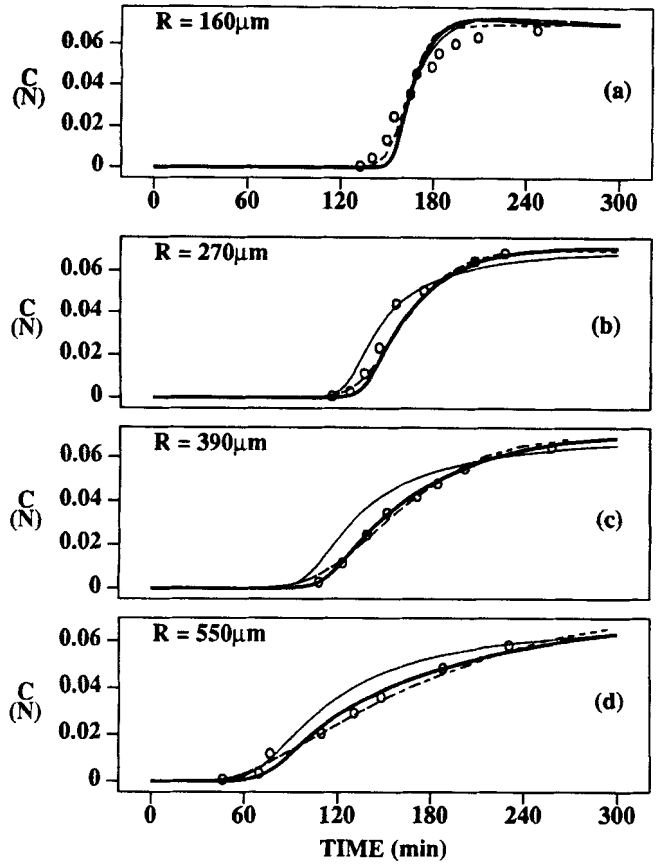

Figure 12. Simulations from pore, surface and parallel diffusion models with breakthrough data of Sr^{++}.

The simulation parameters are listed in Table 7. For the parallel diffusion $D_p = 1.08 \times 10^{-4}$ cm²/min, and $D_s = 2.35 \times 10^{-6}$ cm²/min. Thick solid line: parallel diffusion simulation. Thin solid line: surface diffusion simulation. Dashed line: pore diffusion simulation. Circles: experimental data from Mercer and Ames (1963).

single-diffusion models for design and scale-up. However, in systems where both pore and surface diffusion are significant, an effective pore diffusion coefficient estimated from the pore diffusion model can be greater than Brownian diffusivity if the solute affinity is sufficiently large. In nonlinear systems, the two diffusion mechanisms have distinctly different effects on breakthroughs. Surface diffusion causes pronounced tailing, whereas pore diffusion causes relatively symmetric spreading. In case of parallel diffusion, effective pore diffusion coefficient decreases with increasing concentration, whereas effective surface diffusion coefficient increases with increasing concentration. The single-diffusion models will not be able to give accurate predictions over a wide concentration range, because surface diffusion may dominate at low concentration, whereas pore diffusion may dominate at high concentration. More important and interesting, in multicomponent systems, transport of high-affinity solutes may be dominated by surface diffusion, whereas transport of low-affinity solutes may be dominated by pore diffusion; elution order can change in such parallel diffusion systems. For these reasons, the parallel diffusion model must be used for nonlinear multicomponent chromatography systems.

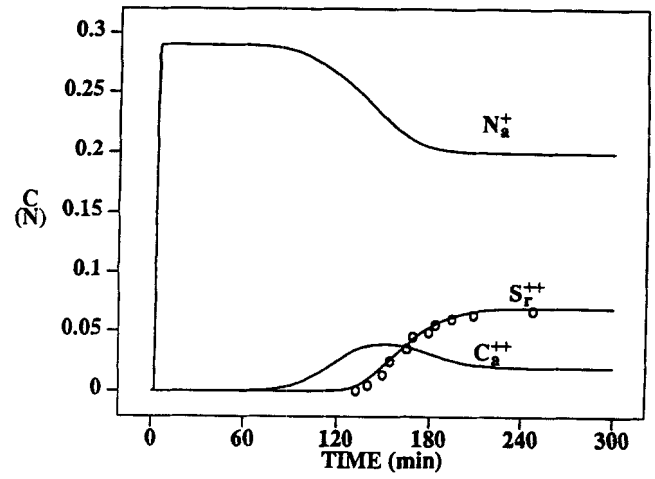

Figure 13. Elution histories of all three ions predicted from the pore diffusion model for the smallest particle size in Figure 12a.

Simulation parameters are the same as in Figure 12 except that the pore diffusion coefficients for all three ions are reduced by 50%.

Acknowledgment

This work was supported in part by a grant from NSF (GER 9024174) and a grant from the Westinghouse Savannah River Company through the DOE Office of Technology Development (TTP#SR#1-3-20-02) in the Underground Storage Tank Integrated Demonstration Program. The authors are grateful for M. V. Ernest's assistance in analyzing the ion exchange data.

Notation

A = Langmuir isotherm constant
B = Langmuir isotherm constant
B_f = Biot number
C_f = dimensionless feed concentration
D_p = intraparticle pore diffusion coefficient
F_r = volumetric flow rate
K = dimensionless equilibrium constant defined in Eq. B2
K_1 = Langmuir isotherm constant
K_2 = isotherm constant defined in Figure 1
K_d = mass action constant
L = column length
N = number of component
N_f = dimensionless film mass-transfer coefficient (Eq. B3)
N_p = dimensionless pore diffusion coefficient
$N_{p_{app}}$ = dimensionless apparent pore diffusion coefficient
N_s = dimensionless surface diffusion coefficient
$N_{s_{app}}$ = dimensionless apparent surface diffusion coefficient
Pe = bulk-phase Peclet number (Eq. B2)
R = particle radius
Y_l = dimensionless adsorption rate
k_a = adsorption rate constant
k_d = desorption rate constant
r = radial position inside a particle
u_0 = average linear interstitial velocity
x = axial position inside column
z = dimensionless axial position inside column (Eq. B1)

Greeks letters

Φ_k = dimensionless adsorption rate constant (Eq. B2)
β = isotherm constant in Figure 1
ϵ_b = column interparticle void fraction
ϵ_p = particle porosity
ξ = dimensionless radial position inside a particle (Eq. B1)

θ = dimensionless solid phase concentration (Eq. 8a)
τ_r = dimensionless retention time

Subscripts

p = quantities associated with pore phase
s = quantities associated with solid phase

Literature Cited

Aris, R., "On the Dispersion of a Solute by Diffusion, Convection, and Exchange between Phases," *Proc. Roy. Soc. London A*, **252**, 538 (1959).

Aris, R., "Interpretation of Sorption and Diffusion Data in Porous Solids," *Ind. Eng. Chem. Fundam.*, **22**, 150 (1983).

Aris, R., and N. R. Amundson, *Mathematical Methods in Chemical Engineering*, Prentice-Hall, Englewood Cliffs, NJ (1973).

Asenjo, J. A., ed., *Separation Processes in Biotechnology*, Marcel Dekker, New York (1990).

Baker, J., *Finite Element Computational Fluid Mechanics*, McGraw-Hill, New York (1983).

Belter, P. A., E. L. Cussler, and W.-S. Hu, *Bioseparations, Downstream Processing for Biotechnology*, Wiley-Interscience, New York (1988).

Berninger, J. A., R. D. Whitley, X. Zhang, and N.-H. L. Wang, "A Versatile Model for Simulation of Reaction and Nonequilibrium Dynamics in Multicomponent Fixed-bed Adsorption Processes," *Comput. Chem. Eng.*, **15**, 749 (1991).

Brecher, L. E., D. C. Frantz, and J. A. Kostecki, "Combined Diffusion in Batch Adsorption Systems Displaying B.E.T. Isotherms: II," *AIChE Symp. Ser.*, **63**, 25 (1967).

Chung, S. F., and C. Y. Wen, "Longitudinal Dispersion of Liquid Flowing through Fixed and Fluidized Beds," *AIChE J.*, **14**, 857 (1968).

Courant, R., and K. O. Friedrichs, *Supersonic Flow and Shock Waves*, Wiley-Interscience, New York (1948).

Cussler, E. L., *Diffusion: Mass Transfer in Fluid Systems*, Cambridge Univ. Press, Cambridge, England (1984).

Crittenden, J. C., B. W. C. Wong, W. E. Thacker, V. O. Snoeyink, and R. L. Hinrichs, "Mathematical Model of Sequential Loading in Fixed-bed Adsorbers," *J. Water Pollut. Control Fed.*, **52**, 2780 (1980).

Dechow, F. J., *Separation and Purification Techniques in Biotechnology*, Noyes, Park Ridge, NJ (1989).

Dedrick, R. L., and R. B. Beckmann, "Kinetics of Adsorption by Activated Carbon from Dilute Aqueous Solution," *AIChE Symp. Ser.*, **63**, 25 (1967).

Do, D., and R. G. Rice, "On the Relative Importance of Pore and Surface Diffusion in Nonequilibrium Adsorption Rate Processes," *Chem. Eng. Sci.*, **42**, 2269 (1987).

Ernest, M. V., Jr., *Development of Ion Exchange Processes for Decontamination of Cesium-137 from Alkaline Nuclear Waste*, School of Chemical Engineering, Purdue Univ., West Lafayette, IN (1994).

Fowler, R., and E. A. Guggenheim, *Statistical Thermodynamics*, Cambridge Univ. Press, Cambridge, England (1960).

Fritz, W., W. Merk, and E. V. Schlünder, "Competitive Adsorption of Two Dissolved Organic onto Activated Carbon: II," *Chem. Eng. Sci.*, **36**, 731 (1981).

Furuya, E., Y. Takeuchi, and K. E. Noll, "Intraparticle Diffusion of Phenols within Bidispersed Macroreticular Resin Particles," *J. Chem. Eng. Japan*, **22**(6), 670 (1989).

Helfferich, F. G., "Ion Exchange Kinetics—Evolution of a Theory," *Mass Transfer and Kinetics of Ion Exchange*, L. Liberti and F. G. Helfferich, eds., NATO ASI Series E: Applied Sciences, No. 71, Nijhoff, The Hague, The Netherlands (1983).

Hu, X., and D. D. Do, "Experimental Concentration Dependence of Surface Diffusivity of Hydrocarbon in Activated Carbon," *Chem. Eng. Sci.*, **49**, 2145 (1994).

Jin, X., J. Talbot, and N.-H. L. Wang, "Analysis of Steric Hindrance Effects on Adsorption Kinetics and Equilibria," *AIChE J.*, **40**, 1685 (1994).

Kapoor, A., R. T. Yang, and A. C. Wong, "Surface Diffusion," *Catal. Rev. Sci. Eng.*, **31**, 129 (1989).

Klein, G., "Calculation of Ideal or Empirically Modified Mass-Action Equilibria in Heterovalent Multicomponent Ion Exchange," *Comput. Chem. Eng.*, **8**, 171 (1984).

Komiyama, H., and J. Smith, "Surface Diffusion in Liquid-Filled Pores," *AIChE J.*, **20**, 1110 (1974).

Kubin, M., "Contribution to the Theory of Chromatography," *Collect. Czech. Chem. Commun.*, **30**, 1104 (1965).

Kucera, E., "Contribution to the Theory of Chromatography Linear Non-equilibrium Elution Chromatography," *J. Chromatog.*, **19**, 237 (1965).

Liapis, A. I., and D. W. Rippin, "A General Model for the Simulation of Multi-component Adsorption from a Finite Bath," *Chem. Eng. Sci.*, **32**, 619 (1977).

Lin, B., Z. Ma, and G. Guiochon, "Influence of Calculation Errors in the Numerical Simulation of Chromatographic Elution Band Profiles using an Ideal or Semi-ideal Model," *J. Chromatog.*, **484**, 83 (1989).

Ma, Z., and G. Guiochon, "Application of Orthogonal Collocation on Finite Elements in the Simulation of Non-linear Chromatography," *Comput. Chem. Eng.*, **15**, 415 (1991).

Mansour, A., D. U. Rosenberg, and N. D. Sylvester, "Numerical Solution of Liquid-Phase Multicomponent Adsorption in Fixed Beds," *AIChE J.*, **28**, 765 (1982).

Mercer, B. W., and L. L. Ames, Jr., *The Adsorption of Cesium, Strontium, and Cerium on Zeolites from Multication Systems*, HW-78461, Hanford Laboratories, General Electric Company, Richland, WA (1963).

Merk, W., W. Fritz, and E. U. Schlunder, "Competitive Adsorption of Two Dissolved Organics onto Activated Carbon-III," *Chem. Eng. Sci.*, **36**, 743 (1980).

Miyabe, K., and M. Suzuki, "Chromatography of Liquid-Phase Adsorption on Octadecylsilyl-Silica Gel," *AIChE J.*, **38**, 901 (1992).

Moynihan, H. J., R. A. Novy, and N.-H. L. Wang, "Analysis of Enzymatic Hydrolysis of Urea in a Single Particle: Effects of pH-dependent Kinetics, Ionic Equilibria, Product Inhibition, and Nernst-Plank Diffusion," *Chem. Eng. Commun.*, **72**, 47 (1988).

Neogi, P., and E. Ruckenstein, "Transport Phenomena in Solids with Bidispersed Pores," *AIChE J.*, **26**, 787 (1980).

Noll, K. E., V. Gounaris, and W.-S. Hou, *Adsorption Technology for Air and Water Pollution Control*, Lewis, Chelsea, MI.

Riekert, L., "The Relative Contribution of Pore Volume Diffusion and Surface Diffusion to Mass Transfer in Capillaries and Porous Media," *AIChE J.*, **31**, 863 (1985).

Robinson, S. M., W. D. Arnold, and C. H. Byers, "Mass-Transfer Mechanisms for Zeolite Ion Exchange in Wastewater Treatment," *AIChE J.*, **40**, 2045 (1994).

Ruthven, D. M., *Principles of Adsorption and Adsorption Processes*, Wiley-Interscience, New York (1984).

Schneider, P., and J. Smith, "Adsorption Rate Constants from Chromatography," *AIChE J.*, **14**, 762 (1968a).

Schneider, P., and J. Smith, "Chromatographic Study of Surface Diffusion," *AIChE J.*, **14**, 886 (1968b).

Suzuki, M., "Notes on Determining the Moments of the Impulse Response from the Basic Transformed Equations," *J. Chem. Eng. Japan*, **6**, 540 (1973).

Suzuki, M., and F. Takao, "Concentration Dependence of Surface Diffusion Coefficient of Propionic Acid in Activated Carbon Particles," *AIChE J.*, **28**, 380 (1982).

Suzuki, M., *Adsorption Engineering*, Elsevier, Amsterdam (1990).

Talbot, J., X. Jin, and N.-H. L. Wang, "New Equations for Multicomponent Adsorption Kinetics," *Langmuir*, **10**, 1663 (1994).

Thacker, W. E., J. C. Crittenden, and V. L. Snoeyink, "Modeling of Adsorber Performance: Variable Influent Concentration and Comparison of Adsorbents," *J. Water Pollut. Control Fed.*, **56**, 243 (1984).

Tilton, R. D., C. R. Robertson, and A. P. Gast, "Lateral Diffusion of Bovine Serum Albumin Adsorbed at the Solid-Liquid Interface," *J. Colloid Interf. Sci.*, **137**, 192 (1990a).

Tilton, R. D., A. P. Gast, and C. R. Roberston, "Surface Diffusion of Interacting Proteins," *Biophys. J.*, **58**, 1321 (1990b).

Van Deemter, J. J., F. F. Zuiderweg, and A. Flinkenberg, "Longitudinal Diffusion and Resistance to Mass Transfer as Causes of Nonideality in Chromatography," *Chem. Eng. Sci.*, **5**, 271 (1956).

Villadsen, J., and M. L. Michelsen, *Solutions of Differential Equations Models by Polynomial Approximation*, Prentice-Hall, Englewood Cliffs, NJ (1978).

Wankat, P. C., *Large-Scale Adsorption Chromatography*, CRC Press, Boca Raton, FL (1986).
Whitaker, S., "Diffusion in Packed Beds of Porous Particles," *AIChE J.*, **34**, 679 (1988).
Whitley, R. D., K. E. Van Cott, and N.-H. L. Wang, "Analysis of Nonequilibrium Adsorption/Desorption Kinetics and Implications for Analytical and Preparative Chromatography," *Ind. Eng. Chem. Res.*, **32**, 149 (1993).
Wilson, E. J., and C. J. Geankoplis, "Liquid Mass Transfer at Very Low Reynolds Numbers in Packed Beds," *Ind. Eng. Chem. Fundam.*, **5**, 9 (1966).
Yeroshenkova, G. V., S. A. Volkov, and K. I. Sakodynskii, "Effect of Packing Irregularities along the Bed Length," *J. Chromatog.*, **262**, 19 (1983).
Yoshida, H., M. Yoshikawa, and T. Kataoka, "Parallel Transport of BSA by Surface and Pore Diffusion in Strongly Basic Chitosan," *AIChE J.*, **40**, 2034 (1994).

Appendix A: Derivation of Pore and Solid Phase Boundary Conditions for the Generalized Nonequilibrium Model

Four boundary conditions are needed for the pore phase and the solid phase mass-balance equations. Symmetric conditions can be used to give two conditions at $r = 0$. Yet, two more conditions are needed at $r = R$. The flux from the liquid phase to the particle phase at the surface $r = R + \Delta R$ can be written

$$J_m(r = R + \Delta R) = k_f[c_b - c_p(r = R + \Delta R)]. \quad \text{(A1)}$$

The pore and surface diffusion fluxes at $r = R$ can be written as

$$J_d(r = R) = -\epsilon_p D_p \left.\frac{\partial c_p}{\partial r}\right|_{r=R} - (1-\epsilon_p) D_s \left.\frac{\partial q}{\partial r}\right|_{r=R}, \quad \text{(A2)}$$

where J_m is the film mass-transfer flux, and J_d is the total diffusional flux. As $\Delta R \to 0$, summation of J_m and J_d has to be zero, since there is no accumulation on the control surface at $r = R$. Then we have

$$\epsilon_p D_p \left.\frac{\partial c_p}{\partial r}\right|_{r=R} + (1-\epsilon_p) D_s \left.\frac{\partial q}{\partial r}\right|_{r=R} = k_f[c_b - c_p(r = R)]. \quad \text{(A3)}$$

One more boundary condition is needed and should be independent of Eq. A3. A control volume, defined between R and $R - \Delta R$, is chosen. Mass balance for the solid phase concentration in the control volume can be written as follows:

$$-4\pi\left[R^2 J_s(r = R) - (R - \Delta R)^2 J_s(r = R - \Delta R)\right] = 4\pi R^2 \Delta R\left[\left.\frac{\partial q}{\partial t}\right|_{r=R} - y_l\right]. \quad (4)$$

The $J_s(r = R - \Delta R)$ of the preceding equation can be expanded as

$$J_s(r = R - \Delta R) = J_s(r = R) - \left.\frac{\partial J_s}{\partial r}\right|_{r=R} \Delta R. \quad \text{(A5)}$$

The spatial derivative of the flux J_s at $r = R$ is zero because there is no surface diffusion outside the particle ($r > R$). Therefore,

$$(R - \Delta R)^2 J_s(r = R - \Delta R) \cong (R - \Delta R)^2 J_s(r = R) = [R^2 - 2R\Delta R + (\Delta R)^2] J_s(r = R). \quad \text{(A6)}$$

Therefore, from Eqs. A4 and A6, we have

$$-R^2 J_s(r = R) + [R^2 - 2R\Delta R + (\Delta R)^2] J_s(r = R) = R^2 \Delta R\left[\left.\frac{\partial q}{\partial t}\right|_{r=R} - y_l\right]. \quad \text{(A7)}$$

By dropping the second-order term, we have

$$-2R\Delta R J_s(r = R) = R^2 \Delta R\left[\left.\frac{\partial q}{\partial t}\right|_{r=R} - y_l\right]. \quad \text{(A8)}$$

Therefore,

$$\frac{\partial q}{\partial t} = y_l + \frac{2D_s}{R}\frac{\partial q}{\partial r}. \quad \text{(A9)}$$

Thus, Eqs. A3 and A9 give the coupled boundary conditions for both pore and solid phase concentrations for the parallel pore and surface diffusion models in the case of nonequilibrium adsorption kinetics. Note that Eq. A9 is equivalent to setting the second-order spatial derivative to zero in the continuity Eq. 5.

Appendix B: Generalized Model in Dimensionless Variables

To simplify the Eqs. 1–7 discussed in the text, we defined the following dimensionless variables,

$$\tau = \frac{tu_0}{L} \qquad z = \frac{x}{L} \qquad \xi = \frac{r}{R} \qquad C_{bi} = \frac{k_{a_i}}{k_{d_i}} c_{bi}$$

$$C_{pi} = \frac{k_{ai}}{k_{di}} c_{pi} \quad \text{(B1)}$$

$$\Phi_{ki} = \frac{(1-\epsilon_p) k_{ai} q_{si} L}{\epsilon_p u_0} \qquad Pe_i = \frac{u_0 L}{E_{bi}} \qquad B_{fi} = \frac{k_{fi} L}{\epsilon_p R u_0}$$

$$K_i = \frac{1-\epsilon_p}{\epsilon_p}\frac{k_{ai}}{k_{di}} q_{si} \quad \text{(B2)}$$

$$N_{fi} = 3\frac{L}{R}\frac{(1-\epsilon_b) k_{fi}}{\epsilon_b u_0} \qquad N_{pi} = \frac{D_{pi} L}{u_0 R^2} \qquad N_{si} = \frac{D_{si} L}{u_0 R^2}. \quad \text{(B3)}$$

The dimensionless equations for the generalized model are thus written as

$$\frac{\partial C_{bi}}{\partial \tau} = \frac{1}{P_{ei}}\frac{\partial^2 C_{bi}}{\partial z^2} - \frac{\partial C_{bi}}{\partial z} - N_{fi}[C_{bi} - C_{pi}(\xi = 1)] \qquad i = 1, 2, \ldots, N \quad \text{(B4)}$$

$$\frac{\partial C_{pi}}{\partial \tau} = N_{pi}\nabla_s^2 C_{pi} - \Phi_{ki} Y_{li} \tag{B5}$$

$$K_i \frac{\partial \theta_i}{\partial \tau} = K_i N_{si}\nabla_s^2 \theta_i + \Phi_{ki} Y_{li}, \tag{B6}$$

where $Y_l = y_l/(q_s k_d)$. The boundary and initial conditions for the mobile phase are

$$\frac{\partial C_{bi}}{\partial z} = \begin{cases} P_{ei}[C_{bi} - C_{fi}(\tau)] & z = 0 \\ 0 & z = 1 \end{cases} \qquad i = 1, 2 \ldots N \tag{B7}$$

$$C_{bi} = C_{bi}(0, z) \qquad i = 1, 2 \ldots, N. \tag{B8}$$

For the pore and the solid phase, the boundary and initial conditions are

$$N_{pi}\frac{\partial C_{pi}}{\partial \xi} + K_i N_{si}\frac{\partial \theta_i}{\partial \xi} = \begin{cases} B_{fi}(C_{bi} - C_{pi}) & \xi = 1 \\ 0 & \xi = 0 \end{cases} \tag{B9a}$$

$$2K_i N_{si}\frac{\partial \theta_i}{\partial \xi} = K_i \frac{\partial \theta_i}{\partial \tau} - \Phi_{ki} Y_{li} \qquad \xi = 1 \quad \tau \in [0, \infty] \tag{B9b}$$

$$\frac{\partial C_{pi}}{\partial \xi} = 0 \qquad \xi = 0, \quad \tau \in [0, \infty] \tag{B10}$$

$$\frac{\partial \theta_i}{\partial \xi} = 0 \qquad \xi = 0, \quad \tau \in [0, \infty] \tag{B11}$$

$$C_{pi} = C_{pi}(\tau, \xi), \qquad \tau = 0, \quad i = 1, 2, \ldots, N \tag{B12}$$

$$\theta_i = \theta_i(\tau, \xi), \qquad \tau = 0 \quad \xi \in [0, 1]. \tag{B13}$$

Appendix C: Derivation of the Local Linearized Kinetic Equation for the Nonequilibrium Pore Diffusion Model

In a single component system, when the adsorption kinetics are slow, $\Phi_k \ll 1$, and if the bed is presaturated with C_p^0 and θ^0, with small perturbations, ΔC_p and $\Delta\theta$, Eq. 8a can be written as

$$y_l^0 = q_s k_d\left(C_p^0 \phi^0 - \theta^0\right) \tag{C1}$$

$$y_l^0 + \Delta y_l = q_s k_d\left\{\left(C_p^0 + \Delta C_p\right)[\phi^0 + \Delta\phi - (\theta^0 + \Delta\theta)]\right\}. \tag{C2}$$

Subtracting Eq. C1 from Eq. C2 and dropping the higher order terms with respect to ΔC_p and $\Delta\phi$, we have the perturbed rate as

$$\Delta y_l = q_s k_d\left[\Delta C_p \phi^0 - \left(1 - C_p^0 \left.\frac{\partial \phi}{\partial \theta}\right|_{C_p^0, \theta^0}\right)\Delta\theta\right]. \tag{C3}$$

Rearranging Eq. C3, we have

$$\Delta y_l = q_s k_d \phi^0 \left(\Delta C_p - \Delta\theta \frac{1 - C_p^0 \left.\frac{\partial \phi}{\partial \theta}\right|_{C_p^0, \theta^0}}{\phi^0}\right). \tag{C4}$$

Note that in the case of equilibrium, the following can be derived from Eq. 8c,

$$\frac{\partial \theta}{\partial C_p} = \frac{\phi}{1 - C_p \dfrac{\partial \phi}{\partial \theta}}. \tag{C5}$$

Equation C4 then becomes

$$\Delta y_l = q_s k_d \phi^0 \left(\Delta C_p - \Delta\theta \frac{1}{\left.\dfrac{\partial \theta}{\partial C_p}\right|_{C_p^0, \theta^0}}\right). \tag{C6}$$

When C_p^0 and θ^0 are zero, $\phi^0 = 1$, Eq. C6 becomes

$$\Delta y_l = q_s k_d(\Delta C_p - \Delta\theta). \tag{C7}$$

Thus, the linear kinetic equation in Schneider and Smith (1968a) is a special case of Eq. C6. Notice at equilibrium,

$$\phi^0 = \frac{\theta^0}{C_p^0}; \tag{C8}$$

therefore, we have,

$$\Delta y_l = q_s k_d \frac{\theta^0}{C_p^0}\left(\Delta C_p - \Delta\theta \frac{1}{\left.\dfrac{\partial \theta}{\partial C_p}\right|_{C_p^0, \theta^0}}\right), \tag{C9}$$

which is the locally linearized kinetic equation.

Manuscript received Apr. 14, 1995, and revision received Aug. 11, 1995.